4th Workshop Of
CODE_BRIGHT USERS

3rd May 2012
Barcelona, Spain

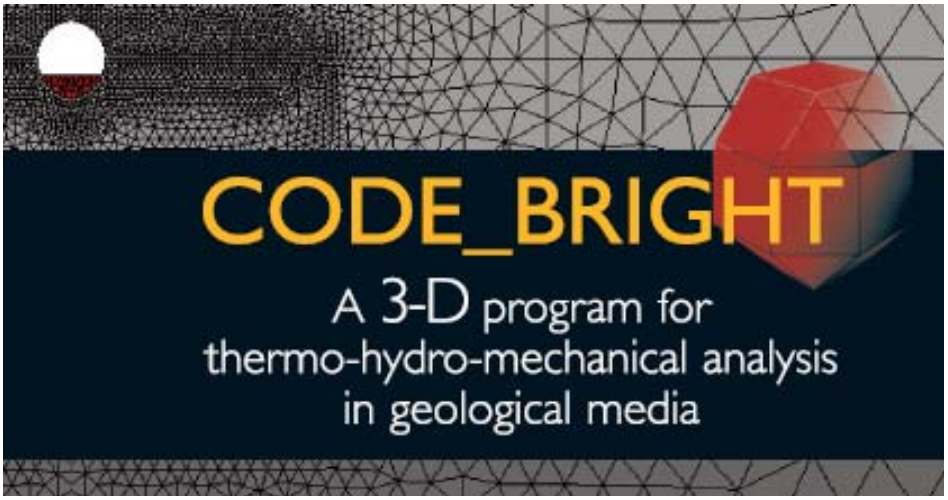

Department of Geotechnical Engineering and Geosciences
(UPC. Barcelona. Spain)
CIMNE
(Centro Internacional de Métodos Numéricos en Ingeniería.
Barcelona. Spain)

CODE_BRIGHT

A 3-D program for thermo-hydro-mechanical analysis in geological media

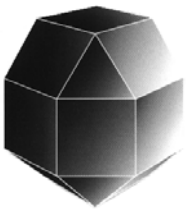

4th WORKSHOP OF CODE_BRIGHT USERS

Barcelona, 3 May 2012

Department of Geotechnical Engineering and Geosciences

(UPC. Barcelona. Spain)

CIMNE

(Centro Internacional de Métodos Numéricos en Ingeniería. Barcelona. Spain)

CONTENTS

Modelling Lasgit in situ experiment
S. Olivella, E.E. Alonso, D. Arnedo & C. Hoffmann

Analysis of convergence of a THM coupled problem
Nubia A. González, Sebastià Olivella & Jean Vaunat

TERMO-MECHANICAL MODELLING OF AN AERIAL CAVERN UNDER CLIMATIC ACTIONS

D. Ruiz[*], J. Vaunat[*], S. Samat[*] and D. Virely[†]

[*] Department of Geotechnical Engineering and Geosciences
Technical University of Catalonia (UPC)
Campus Norte UPC, 08034 Barcelona, Spain
E-mail: daniel.ruiz@upc.edu
[†] Laboratoire Régional des Ponts et Chaussées, France

Key words: Climatic Actions, Radiation, Heat, Cliff, Cavern, Failure, Displacement

Abstract. *This paper presents the modelling of a particular case under climatic actions; specifically it is a calcareous cliff exposed to solar radiation and changes in air temperature. Due to recent failure of the roof within cavern (2010) situated at mid-height of the cliff was generated an investigation through instrumentation within and above it. The interpretation is performed with the help of a general model for the coupled analysis of flow (air) and heat transfer in the rock, including a special handling of the surface in contact with the atmosphere.*

1 INTRODUCTION

The interactions between the ground and the atmosphere play a central role in the analysis of the natural risks associated to geotechnical failures. Soil-atmosphere interaction is a complex phenomenon that involves balance of heat and different species (liquid water, vapour, air) across the soil surface. Such an interaction has been implemented in CODE_BRIGHT by means of a specific boundary conditions (Noilan & Planton, 1989) that impose varying fluxes of evaporation, rainfall, radiation and heat together with changes in atmosphere pressure and temperature. Of particular relevance are the fluxes due to evaporation (E*v*) and radiation (R*n*), usually not considered in classical geotechnical applications.

The objective of the paper is to present a model able to simulate the effect of climate on slopes and to analyze with it real case; it is an instrumented cliff that contains a troglodyte cavity with roof stability problems. The analysis aims at understanding the mechanisms responsible of the current deformation of the cliff and its effect on cavity roof stability. As the rock is considered dry, deformations are essentially due to the thermal load caused by solar radiation and changes in air temperature. This case is used to validate, by comparison with field data, the equations for radiation and thermo-mechanical coupling, as well as to provide insights into the stability of fractured rock exposed to the atmosphere.

2 MODELLING CLIMATIC ACTIONS

The processes controlling atmosphere conditions include effects of radiation and heat exchange, moist processes (clouds and precipitation), air mass motion and interactions with earth ground components (free surface water, vegetation, outcropping soils and rocks). Figure 1 presents a schematic overview of these different effects and their interactions. The soil-atmosphere interaction is due to boundary fluxes like a precipitation (P), evaporation (E) and solar radiation (Rn) that affect the balance in the thermo-hydro-mechanical model.

The Thermo-hydro-mechanical processes in soils and rocks fulfilled basic laws of physics, in that case the conservation laws of mass, energy and the stress equilibrium.

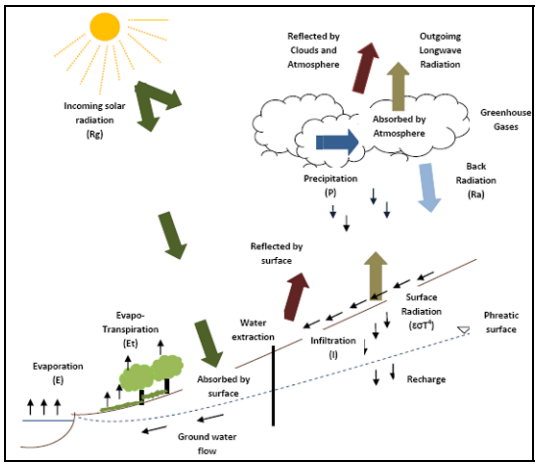

(adapted after Blight, 1997)

Figure 1: Schema of mass and energy interactions between ground, vegetation and atmosphere.

In unsaturated conditions, soils and rocks are composed by a solid skeleton filled by two fluid species: air and water. The latter are present either in liquid state (liquid water and dissolved air) or under the form of gas (vapour and dry air).

The general model for the coupled analysis is governed by the conservation laws of three flows (water (1), air (2), energy (3)) and the stress equilibrium (4) (Vaunat et al., 2012).

$$\frac{Dm_w}{Dt} + div(j_w) = f_w \qquad (1)$$

$$\frac{Dm_a}{Dt} + div(j_a) = f_a \qquad (2)$$

$$\frac{De}{Dt} + div(j_e) = f_e \qquad (3)$$

$$div\ \sigma + \rho g = 0 \qquad (4)$$

In this particular case (Roche Gageac) in absence of water, the heat exchange fluxes at soil surface are:

- Solar direct radiation (short wave, inflow).
- Radiation re-emitted by the atmosphere (long wave, outflow).
- Radiation re-emitted by the rock (outflow).
- Heat conduction due to temperature gradient between the rock and the atmosphere.
- Heat convected by the wind.

The total heat flux (R_n) and radiation (R_g , R_a) flux has been simulated using the equations (5), (6) and (7).

$$R_n = (1 - A_l)R_g + \varepsilon R_a - \varepsilon\sigma T_0^{\ 4} + H_s \qquad (5)$$

$$R_g = \frac{\pi R_{g0}}{2 d_s} \sin\left(\frac{(t - t_m + 0.5 d_s)\cdot\pi}{d_s}\right) \qquad (6)$$

$$R_a = \sigma(T_a)^4\left(0.605 + 0.048\sqrt{1370\cdot\rho_{va}}\right) \qquad (7)$$

3 NUMERICAL MODELLING OF AN AERIAN CAVERN – LA ROCHE GAGEAC

The site concerns a calcareous cliff of Cretaceous age, located in the valley of Dordogne river, France. The cliff culminates at a height of about 100 m above the village of “La Roche Gageac” and is prone to block falls. Several events occurred during the last century (1920, 1954 and 1994). The present study deals with a recent failure that occurs during the winter 2010. It involves a troglodyte cavern, situated at mid-height of the cliff above an old fortification used as refuge during the Hundred Year’s war and now recognized as a touristic site. Part of the roof fell within the cavern, endangering the historical monument and leaving a rock beam of questioning stability at the crown of the cavern (Figure 2). The concern about the possible failure of the beam that may, on the one hand, damage irremediably the historical structure and push the

existing debris outside the cavern on top of the village, and, on the other hand, affect the stability of the upper face of the cliff, led to the installation of a detailed displacement survey within and above the cavern.

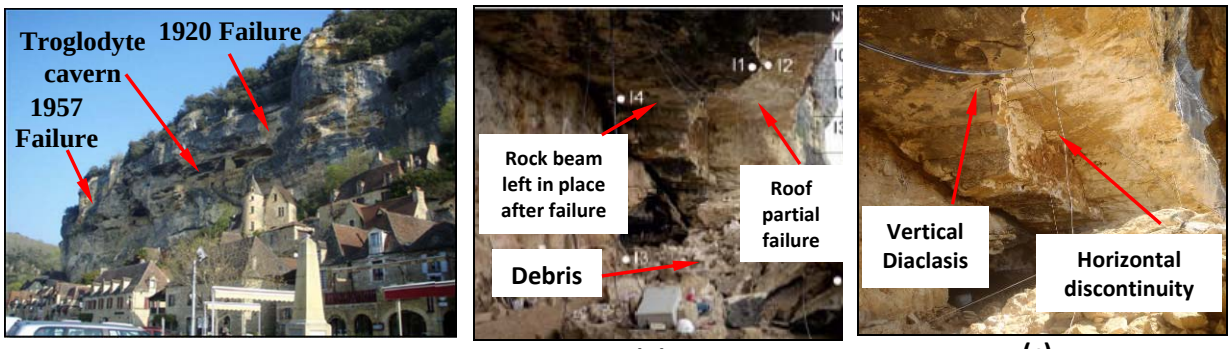

Figure 2: a) General view of the cliff; b) General view of the cavern; c) Beam left in place after the failure

Two main families of discontinuities are observed in the massif, possibly controlled by stress release during valley formation and major tectonics directions: 1) a family of decametre-spaced, decimetre wide open fractures oriented parallel to the cliff face and 2) a family of vertical diaclases of millimetre to centimetre width that cut orthogonally the fractures. Opening between essentially horizontal stratification planes and superficial flaking can be observed in the decompression zones above the cavern.

The survey focuses on displacement and temperature monitoring in the cavern and on the cliff upper face. Fissurometers provide relative displacements across the discontinuities delimiting the rock beam within the cavern. Two extensometers provided with thermal sensors and installed in boreholes drilled horizontally from the cliff face above the cavern (D1 and D2) allow to follow-up displacements and temperature at 2, 4 and 6 m in depth in the rock. Meteorological data are available at a station located at 10 km from the site. (Figure 3).

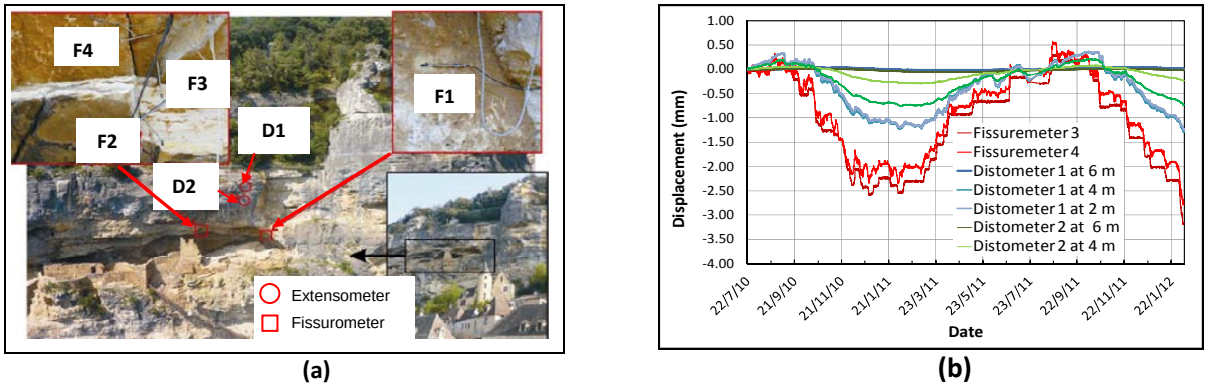

Figure 3: a) Detail of the instrumentation; b) Displacement registers in the extensometers and the fissurometers.

The Figure 3 shows that displacements of fissurometers are larger than in distometer by temperature effect.

3.1 Numerical Model

To support the interpretation of instrumentation, a numerical has been built to analyze the mechanisms at the basis of the time evolution of displacements and, particularly, of its relationship with temperature. The numerical model considers a vertical section of the cliff passing through the diaclasis previously mentioned (see Fig. 15). Boundaries within the massif

have been set at 100 m from cliff face and top, respectively to avoid possible influence on the computation.

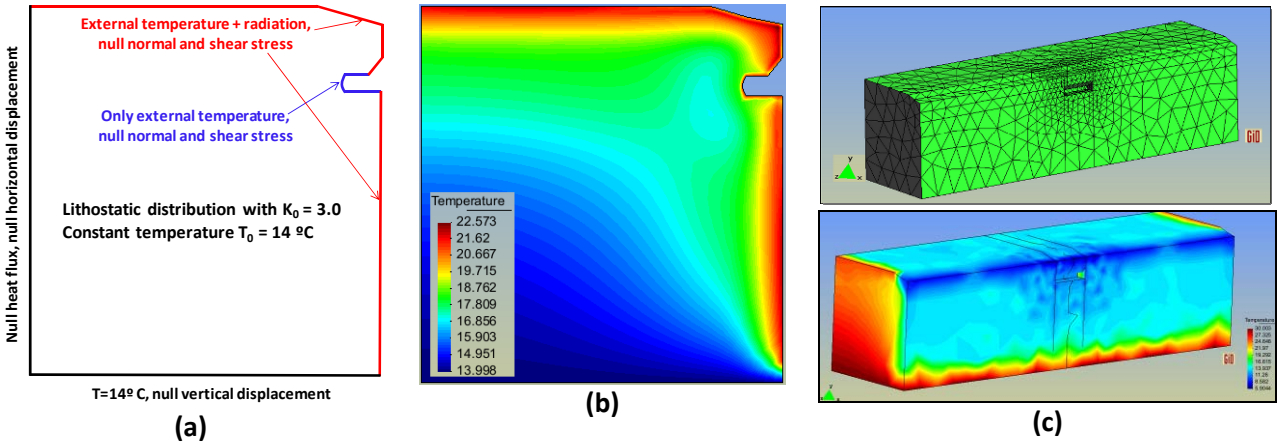

Figure 4: a) Geometry. Initial boundary; b) Temperature Model 2D; c) Temperature Model 3D

From the initial models (2D and 3D) in which the mechanical model is elastic and including daily atmospheric temperature and solar radiation (both short-wave and long-wave) is simulated the response of the distometers in temperature and displacement (Figure 4). These results shows that the rock mass has an elastic behavior and the diaclasis and discontinuities may be irreversible deformations due to the temperature effect.

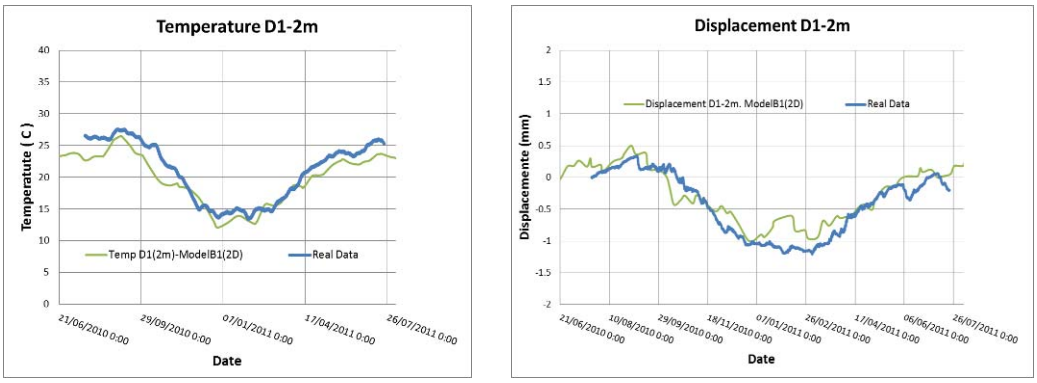

Figure 5: a)Temperature Distometer 1 – 2m ; b) Displacement Distometer 1 – 2m

4 CONCLUSIONS

- The numerical model shows the possibility of quantitatively three dimensional problems of interactions soil-atmosphere by using a boundary condition specific for this process.
- In the preliminary analysis presented in this paper is validated the soil-atmosphere model through the comparison with instrumentation and field data.
- For complete case analysis is necessary to consider areas of surface degradation and a decompression area at the roof of the cave.

REFERENCES

J. Noilan and S. Planton, 1989. A Simple Parameterization of Land Surface Processes for Meteorological Models. Montly Weather Review, vol 117, pp 536-549.

S. Samat and J. Vaunat 2011. Enviromental Actions On Slope Responses. 3rd Workshop of CODE_BRIGHT USERS.

EXTENSION OF CODE_BRIGHT TO SIMULATE NON-ISOTHERMAL CO_2 INJECTION IN DEEP SALINE AQUIFERS

Victor Vilarrasa[1,2], Sebastia Olivella[2], Orlando Silva[3] and Jesus Carrera[1,3]

[1] GHS, Institute of Environmental Assessment and Water Research (IDÆA), CSIC, Jordi Girona 18-26, 08034 Barcelona, Spain
[2] Dept Geotechnical Engineering and Geosciences, Technical University of Catalonia (UPC-BarcelonaTech), Jordi Girona 1-3, 08034 Barcelona, Spain
[3] Fundación Ciudad de la Energía (CIUDEN), CO_2 Geological Storage Programme, II Av. de Compostilla 2, 24400 Ponferrada (León), Spain

INTRODUCTION

Carbon dioxide (CO_2) permanent storage in deep geological formations is considered a promising solution for mitigating greenhouse gas emissions to the atmosphere. Pressure (*P*) and temperature (*T*) conditions of deep geological formations suitable for storing CO_2 are such that this greenhouse gas remains in a dense state, i.e. liquid or supercritical (SC). In fact, in the conventional CO_2 storage it is usually assumed that CO_2 will reach the aquifer in SC conditions. However, CO_2 may not be in thermal equilibrium with the medium when it enters the aquifer because pressure and temperature injection conditions at the wellhead can be diverse and CO_2 will not equilibrate with the geothermal gradient if the flow rate is high. Therefore, modeling of CO_2 injection and storage should take into account non-isothermal two-phase flow processes.

CO_2 density will be lower than that of the resident brine at the *P* and *T* conditions at which CO_2 can enter in deep saline formations. Therefore, it will flow along the top of the aquifer because of buoyancy. Thus, suitable aquifers should be capped by a low-permeability rock to avoid CO_2 migration to shallower aquifers and the ground surface. Actually, this is one of the main concerns in CO_2 permanent storage, i.e. to ensure the caprock mechanical stability to avoid CO_2 leakage.

CO_2 injection can result in significant pressure buildup, which affects the stress field and may induce large deformations (Vilarrasa *et al*., 2010b; 2011). These can eventually damage the caprock and open up new flow paths. Moreover, the thermal disequilibrium between the injected CO_2 and the aquifer can induce additional stress changes that may affect the caprock stability. We have extended the finite element numerical code CODE_BRIGHT (Olivella *et al*., 1994; 1996) to simulate non isothermal CO_2 injection and storage into deep saline aquifers.

IMPLEMENTATION OF CO_2 PROPERTIES IN CODE_BRIGHT

To simulate non-isothermal CO_2 injection some subroutines of CODE_BRIGHT were extended by implementing specific thermodynamic functions and fluid properties relationships. The CO_2 density was calculated through the Redlich and Kwong (1949) equation of state (EOS) with the parameters proposed for CO_2 by Spycher *et al*. (2003). This EOS is a cubic equation in the form of

$$V^3 - \left(\frac{RT}{P_g}\right)V^2 - \left(\frac{RTb}{P_g} - \frac{a}{P_g\sqrt{T}} + b^2\right)V - \left(\frac{ab}{P_g\sqrt{T}}\right) = 0\,, \qquad (1)$$

where *V* is the molar volume of the CO_2, *R* is the gas constant, *T* is temperature, P_g is CO_2 pressure and *a* and *b* represent measures of intermolecular attraction and repulsion, respectively. Note that if $a = b = 0$, the ideal gas law is recovered.

Given a CO_2 pressure P_g and a temperature *T*, Eq. (1) can be solved directly for *V* following a method like the one proposed by Nickalls (1993).

Once the molar volume V is known, the CO_2 density, ρ_g, is calculated as

$$\rho_g = \frac{M_{CO2}}{V}, \tag{2}$$

where $M_{CO2} = 0.044$ kg/mol is the CO_2 molecular weight.

CO_2 viscosity has been taken from Altunin and Sakhabetdinov (1972). These expressions for CO_2 density and viscosity are valid regardless of the temperature and pressure conditions (Figure 1). Additionally, water density increase due to CO_2 dissolution has been implemented following Garcia (2003).

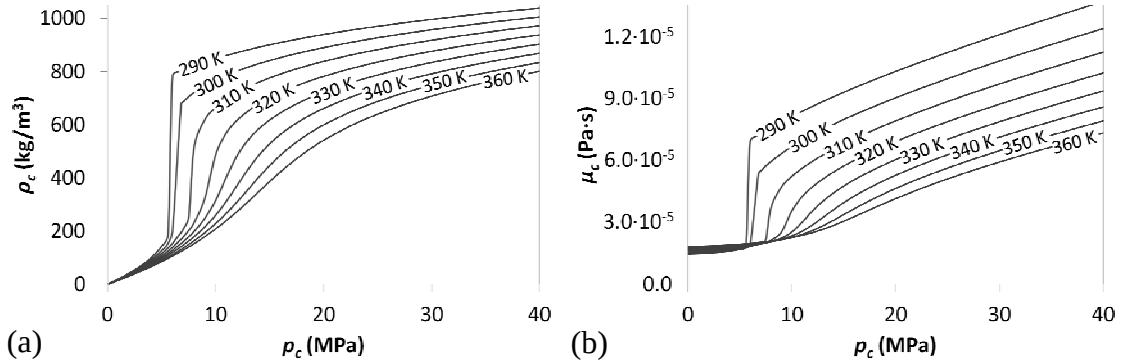

Figure 1. (a) CO_2 density and (b) viscosity as a function of pressure for several temperatures.

The specific enthalpy of CO_2, h_g, can be evaluated integrating the fundamental thermodynamic relation

$$\mathrm{d}\,h_g = c_p\,\mathrm{d}\,T + \left[V - T\left(\frac{\partial V}{\partial T}\right)_p\right]\mathrm{d}\,P_g, \tag{3}$$

where c_p is the specific heat capacity at constant pressure. Integrating Eq. (3) at constant temperature between a reference pressure, e.g. atmospheric pressure, and the CO_2 pressure P_g yields

$$h_g\left(P_g,T\right) - h_g^*\left(T\right) = \int_0^{p_g}\left[V - T\left(\frac{\partial V}{\partial T}\right)_p\right]\mathrm{d}\,P_g, \tag{4a}$$

or

$$h_g\left(P_g,T\right) - h_g^*\left(T\right) = RT\left(Z-1\right) + \int_\infty^V\left[T\left(\frac{\partial P_g}{\partial T}\right)_V - P_g\right]\mathrm{d}V, \tag{4b}$$

where h_g^* is the enthalpy of an ideal gas at atmospheric pressure, which only depends on temperature. Adopting the Redlich-Kwong EOS with the parameters proposed by Spycher *et al.* (2003), Eq. (4) becomes

$$h_g\left(P_g,T\right) - h_g^*\left(T\right) = \left(P_gV - RT - \frac{1.5a - a_1T}{\sqrt{T}b}\ln\left(1+\frac{b}{V}\right)\right)/M_{CO2}, \tag{5}$$

where temperature expressed in K, molar volume in m^3/mol and gas pressure in Pa gives enthalpy in J/kg. We also account for the enthalpy of dissolved CO_2, according to Han *et al.* (2010).

Once the CO_2 enthalpy is determined through Eq. (5), the CO_2 specific heat capacity can be calculated from its definition

$$c_p = \left(\frac{\partial h_g}{\partial T} \right)_p . \tag{6}$$

Applying Eq. (6) with the expression of the enthalpy given by Eq. (5) yields

$$c_p = \frac{\partial h^*(T)}{\partial T} + \left(P_g \frac{\partial V}{\partial T} - R + \frac{0.75a}{b\sqrt{T^3}} \ln\left(1 + \frac{b}{V}\right) + \frac{1.5a - a_1 T}{\sqrt{T}(V+b)V} \frac{\partial V}{\partial T} \right) / M_{CO2}, \tag{7}$$

where

$$\frac{\partial V}{\partial T} = \frac{RV^2 + V\left(Rb - (0.5a - a_1 T)/\sqrt{T^3}\right) - b(0.5a - a_1 T)/\sqrt{T^3}}{3V^2 P_g + 2VRT + RTb - a/\sqrt{T} + b^2 P_g}, \tag{8}$$

where temperature expressed in K, molar volume in m^3/mol and gas pressure in Pa gives the specific heat capacity in J/kg/K. Figure 2 displays the CO_2 enthalpy calculated from Eq. (5) and the CO_2 specific heat capacity calculated from Eqs. (7) and (8).

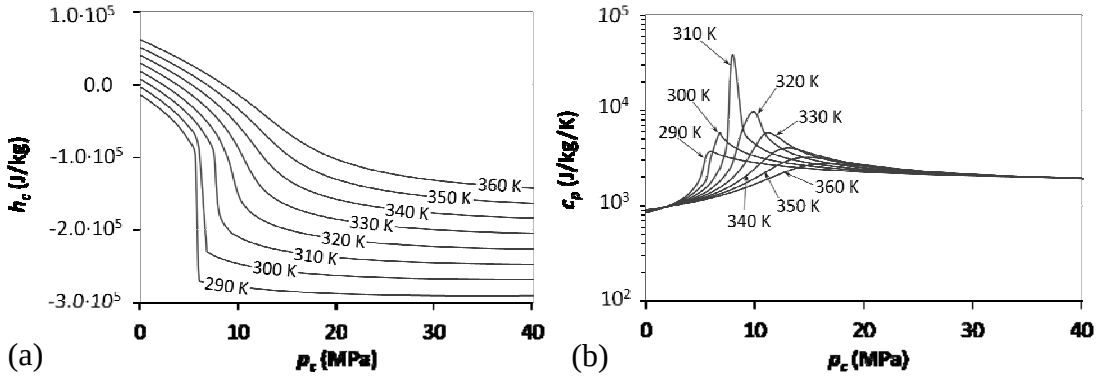

Figure 2. (a) CO_2 enthalpy and (b) CO_2 specific heat capacity as a function of pressure for several temperatures.

MODEL SETUP

We simulated the non-isothermal CO_2 injection in a deep saline aquifer using an axisymmetric model. The aquifer is overlaid and underlain by a 200 m thick seal. The top of the 100 m thick aquifer is located at a depth of 1500 m (55 ºC at the top of the aquifer). The aquifer permeability is 10^{-13} m^2 and its porosity 0.1. Thermal properties are assumed to be the same in both materials. 1 Mt/yr of CO_2 is injected at 20 ºC (cold CO_2). The mesh is made of structured quadrilateral elements, which grow in size for increasing distances to the injection well.

RESULTS

The shape of a CO_2 bubble resulting from an isothermal CO_2 injection is characterized by gravity override (Vilarrasa *et al.*, 2010a). When injecting cold CO_2, which is denser than SC CO_2, this gravity override still applies. However, the density difference between CO_2 and brine becomes much smaller. Therefore, gravity forces lose strength in front of viscous forces, leading to a steeper CO_2-brine interface close to the injection well. Nevertheless, farther away, where CO_2 stays in thermal equilibrium with the aquifer, the shape is very similar in both cases.

Once cold CO_2 enters in the aquifer, both the brine and the rock heat it until they reach thermal equilibrium. Therefore, as the CO_2 bubble grows CO_2 will remain cold around the injection well, but will equilibrate thermally with the aquifer as it moves far away from the well. The thermal transition is abrupt. Furthermore, there is a slight temperature increase due to CO_2 dissolution into the brine, which is an exothermal reaction.

As far as injection pressure is concerned, it is reduced when injecting cold CO_2 instead of SC CO_2 because a CO_2 density increase reduces the volumetric flow rate and therefore the pressure buildup. This is energetically advantageous, because a smaller compression work has to be done to inject the same amount of CO_2. Furthermore, the overpressure in the whole aquifer becomes smaller, which may improve the mechanical stability of the caprock.

CONCLUSIONS

The thermo-hydro-mechanical finite element numerical code CODE_BRIGHT has been extended to simulate non-isothermal CO_2 injection into deep saline aquifers. CO_2 properties are highly dependent on pressure and temperature, especially close to the critical point, which complicates the calculations. We cover both sub and supercritical conditions. We have simulated non-isothermal CO_2 injection in a deep saline aquifer satisfactorily. Including thermal processes in the modeling showed that these induce changes in the hydrodynamic behavior of the CO_2 bubble compared to isothermal CO_2 injection.

ACKNOWLEDGEMENTS

V.V. wishes to acknowledge the Spanish Ministry of Science and Innovation (MCI), through the “Formación de Profesorado Universitario”, and the “Colegio de Ingenieros de Caminos, Canales y Puertos – Catalunya” for their financial support. Additionally, we would like to acknowledge the Spanish Government (Ministry of Industry, Tourism and Trade) through the CUIDEN foundation (project ALM/09/18; www.ciuden.es) and the ‘MUSTANG’ project (from the European Community’s Seventh Framework Programme FP7/2007-2013 under grant agreement nº 227286; www.co2mustang.eu) for their financial support.

REFERENCES

Altunin, VV and Sakhabetdinov, MA (1972). Viscosity of liquid and gaseous carbon dioxide at temperatures 220-1300 K and pressure up to 1200 bar. *Teploenergetika*, 8:85-89.

Garcia, JE (2003). Fluid Dynamics of Carbon Dioxide Disposal into Saline Aquifers. PhD thesis, University of California, Berkeley.

Han, WS, Stillman, GA, Lu, M, Lu, C, McPherson, BJ and Park, E (2010). Evaluation of potential nonisothermal processes and heat transport during CO_2 sequestration. *Journal of Geophysical Research*, 115, B07209, doi: 10.1029/2009JB006745.

Nickalls, RWD (1993). A new approach to solving the cubic: Cardan’s solution revealed. *Math. Gazette*, 77:354-359.

Olivella, S, Carrera, J, Gens, A and Alonso EE, (1994). Non-isothermal multiphase flow of brine and gas through saline media. *Transport In Porous Media*, 15:271–93.

Olivella, S, Gens, A, Carrera, J and Alonso EE, (1996). Numerical formulation for a simulator (CODE_BRIGHT) for the coupled analysis of saline media. *Eng. Computations*, 13:87–112.

Redlich, O and Kwong, JNS (1949). On the thermodynamics of solutions. V. An equation of state. Fugacities of gaseous solutions. *Chem. Rev*. 44:233-244.

Spycher, N, Pruess, K and Ennis-king, J (2003). CO_2-H_2O Mixtures in the Geological Sequestration of CO_2. I. Assessment and calculation of mutual solubilities from 12 to 100°C and up to 600 bar. *Geochim. Cosmochim. Acta*, 67:3015-3031.

Vilarrasa, V, Bolster, D, Dentz, M, Olivella, S and Carrera, J, (2010a). Effects of CO_2 Compressibility on CO_2 Storage in Deep Saline Aquifers. *Transport In Porous Media*, 85(2):619-639.

Vilarrasa, V, Bolster, D, Olivella, S and Carrera, J, (2010b). Coupled Hydromechanical Modeling of CO_2 Sequestration in Deep Saline Aquifers. *International Journal of Greenhouse Gas Control*, 4(6):910-919.

Vilarrasa, V, Olivella, S and Carrera, J (2011). Geomechanical stability of the caprock during CO_2 sequestration in deep saline aquifers. *Energy Procedia*, 4: 5306-5313.

UNDRAINED LOADING AND COLLAPSE OF UNSATURATED SOILS DURING CENTRIFUGE TESTING. AN EXPERIMENTAL AND NUMERICAL STUDY.

Francesca Casini[*], Jean Vaunat[*]

[*] Department of Geotechnical Engineering and Geosciences
Technical University of Catalonia (UPC)
Campus Norte UPC, 08034 Barcelona, Spain
e-mail: francesca.casini@upc.edu

Key words: centrifuge tests, unsaturated soils, undrained loading

Abstract: *The paper presents the results of a centrifuge model of a shallow foundation relying of a layer of unsaturated soil and submitted to axial load for different water level. The objective of the work was to represent a foundation of 1.5 m in diameter on a 15 m soil layer. The model of foundation was a circular disk of 30 mm in diameter and the layer was a cylindrical container of 300 mm in diameter and height. In order to maintain similitude between prototype and model the tests were carried out at 50g. The tests were carried out at the LCPC facilities in Nantes (France). The tested material is an eolian silt from Jossigny, East of Paris. In order to decide the initial conditions of the model in terms of water content and void ratio it was performed a preliminary laboratory investigations. As the intention of the study was to examine the behaviour of a collapsible soil therefore it was decided to prepare the model with a low dry density (14.5 kN/m^3). The evolution of pore water pressure during the tests are compared with the numerical simulation of the prototype with code bright.*

1 INTRODUCTION

The study of unsaturated state on the behaviour of a shallow foundation is an important issue. The state of partial saturation play a foundamental rule on the behaviour of the shallow foundation at failure. The objective of the study was to provide experimental data on the effect of suction (unsaturated soil) on the behaviour of a shallow foundation and to validate numerical results for the case of a foundation relying over a layer of unsaturated silt and submitted to axial load for different water levels.

The tested material is a low plasticity silt with clay. Jossigny silt has a liquid limit w_L = 32.3%, a plastic limit w_P = 17%, 25% of particles less than 2 μm and a unit weight of solid particles γ_s = 26.4 kN/m^3. In order to study the effects of wetting at different initial void a series of oedometric tests has been performed for vertical stress σ_v=200 kPa representing a point in the lower part of the prototype.
The deformation induced by wetting are reported as function of initial dry density in Figure 1.
As the objective of the study was to examine the behaviour of a collapsible soil therefore it was decided to prepare the model with a low dry density (14.5 kN/m^3) and band w= 13% (Sr≅42%).
The soil water retention curve has been obtained under suction controlled condition for different void ratios. In Figure 2 are reported the curve obtained in oedometer cell under suction controlled conditions; the branch of SWRC obtained by Mercury Intrusion Porosimetry on a samples compacted at the dry unit weight of 14.5 kN/m^3 and the point obtained from equalization stage in oedometer and triaxial cell (Casini et al 2012[i]). It was

decided to prepare the sample at a Sr≅42% (e_0=0.82) which correspond a suciotn s≅200 kPa so all the point follows the wetting branch of soil water retention curve when the sample is connected with the water at base in order to avoid the effects of hysteresis

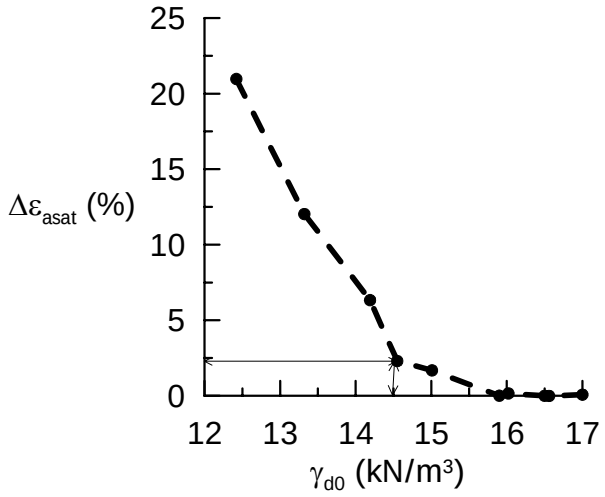

Figure 1 Deformation at saturation- initial dry unit weight.

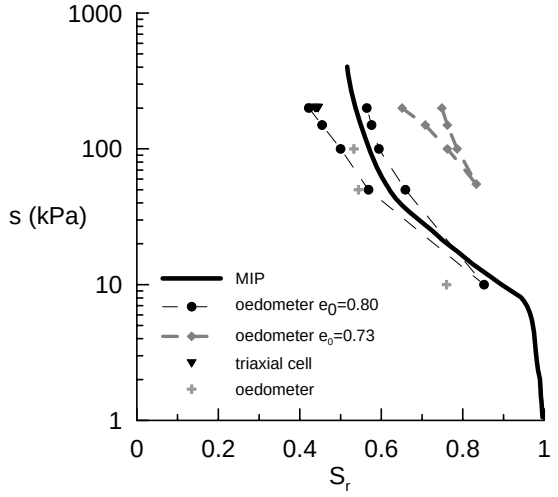

Figure 2 SWRC obtained at different void ratios

2 EXPERIMENTAL APPARATUSES

The samples was compacted statically in a cylindrical container using a 5.0 ton load frame. The procedure set-up used it was the same of previous campaigns performed at ENPC (Cui et al.2005[ii]). It have been prepared in total eight samples (each one weight 35 kg), the properties are reported in table 2 (Casini et al. 2012 in prep[iii].).

Sample	*w (%)*	γ_d *(kN/m3)*	σ_{vc} *(kPa)*	Laboratory
F-1	13.17	14.36	296	ENPC
F-2	16.85	14.12	65	ENPC
I-A	13.9	14.30	189	LCPC
I-B	13.28	14.24	220	LCPC
I-C	13.75	14.54	196	LCPC
II-D	13.75	14.44	208	LCPC
II-E	15.1	14.29	180	LCPC
II-F	12.54	14.57	215	LCPC

Table 2. After compaction properties of the samples used in the centrifuge

In Figure 3 is reported the instrumentation and its position on the sample. It was installed six tensiometers (five in the first campaign) on the diametral opposite sides. Three tensiometers provided by CERMES (labelled ENPC) and three provided by Durham University (labelled DU) in the figures. The elevation are reported in the figure 3. One water pressure transducer was installed at the base of metallic container in the sandy layer in order to control the water pressure in the model.

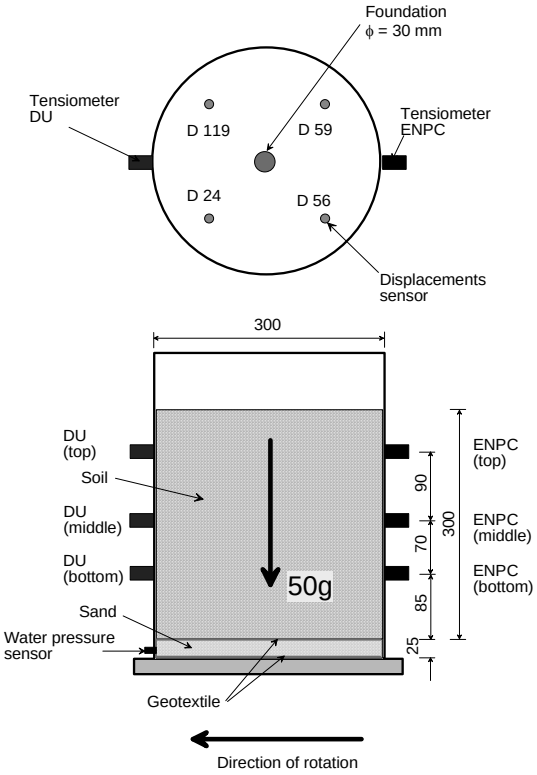

Figure 3. Instrumentation on the sample in centrifuge.

A circular metallic disk (foundation) has been put in the centre of the sample. Load was applied through a spherical hinge to avoid any overturning moment and eccentricity. The load of foundation was performed at a constant displacement rate and the resulting load measured by a load cell. Four LVDT allowed for measuring the vertical displacements at the top of the sample along four radii regularly distributed around the axis of foundation at a distance close to 10 cm (one alone at a distance close to 3 cm in the second campaign).

3 RESULTS

The load of foundation was performed for three height of water level. Defined H_w the height of water level measured from bottom of layer, H the height of layer (Figure 4), the load of foundation was performed for H_w=H, H_w =H/2 and H_w=0.

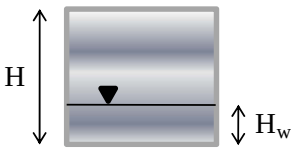

Figure 4. Water level in the model

The evolution of pore water pressure and displacement measured during the test D, are reported in Figure 5 with the comparison with the prediction of a FEM analysis performed with code_bright using the Barcelona Basic Model. An attempt to simulate the effect of increasing the gravity acceleration from 1g to Ng, with N=50 is also perfomed.

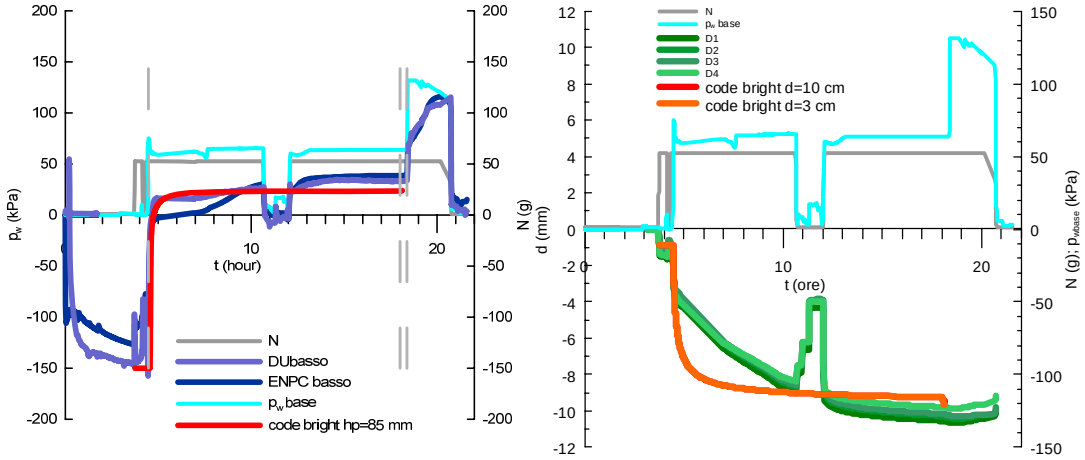

Figure 5. Pore water pressure and displacement evolution during test D.

4 CONCLUSIONS

The results of the centrifuge tests performed on an unsaturated layer of silty soil are presented. The evolution of pore water pressure and displacement are compared with the numerical simulation performed with code_bright. The simulation agree quite well with the measurement. An attempt to simulate the effect of changing the gravity acceleration from 1g to Ng is also performed in order to reproduce the change in suction measured putting in flight the sample and stopped it.

REFERENCES

[i] Casini, F., J. Vaunat, E. Romero, A. Desideri, 2012. Consequences on water retention properties of double porosity features in a compacted silt. Acta Geotechnica, DOI 10.007/s11440-012-0159-6, pp:1-12.

[ii] Chiu C.F., Cui Y.J., Delage P., De Laure E., Haza E. 2005. Lessons learnt from suction monitoring during centrifuge modeling. Proc. of Advanced Experimental Unsaturated Soil Mechanics (EXPERUS 2005), Trento, Italy: 3-8.

[iii] Casini, F., Muñoz, J.J., Lourenço, S., Pereira, J.M., Vaunat, J., Delage, P., Alonso, E., Thorel, L., J. Garnier, J., Gallipoli, D. and Toll, D. Centrifuge investigations on an unsaturated compacted silt: applications to collapse behaviour and to shallow foundations

A METHOD FOR INCORPORATING CHEMICAL REACTIONS INTO CODE_BRIGHT

M. W. Saaltink[1], V. Vilarrasa[1,2], F. De Gaspari [1,2], O. Silva[3] and J. Carrera[2,3]

[1] GHS, Department of Geotechnical Engineering and Geosciences, Technical University of Catalonia (UPC-BarcelonaTech), Barcelona, Spain

[2] Institute of Environmental Assessment and Water Research (IDÆA, CSIC), Barcelona, Spain

[3] Fundación Ciudad de la Energía (CIUDEN), CO_2 Geological Storage Programme, Ponferrada (León), Spain

Key words: Reactive transport, Multiphase flow, CO_2 geological storage

Abstract. *We developed a methodology for incorporating chemical reactions into CODE_BRIGHT. It is limited to chemical systems that can be calculated as a function of the state variables of CODE_BRIGHT (e.g. liquid pressure, gas pressure, temperature). It consists of calculating the chemical composition of this system as a function of these state variables by means of chemical speciation codes and redefining the components of CODE_BRIGHT (e.g., water, air). Hence, the same numerical method can be used for solving the resulting non-linear partial differential equations as the one that already exists in CODE_BRIGHT, that is, a fully coupled Newton-Raphson approach. We applied this methodology to model CO_2 injection into a saline aquifer containing calcite. The model could simulate well the interaction between the development of the CO_2 bubble, dissolution of CO_2 into the brine, calcite dissolution and density dependent flow.*

1 INTRODUCTION

CODE_BRIGHT can handle multiphase flow, heat transport, mass transport, and deformation. Precipitation-dissolution is possible, but limited to one mineral (halite), composed of a single species (dissolved halite). The dissolution of a gaseous species (air) into water only applies to species without further reactions[i]. For some cases this may be a serious limitation. For instance, gaseous CO_2 can dissolve in water and by reacting with the water form acids that dissolve minerals, such as calcite.

We propose a methodology to incorporate more complex chemical reactions into CODE_BRIGHT. We first give a short description of the methodology. Then, we present a model of CO_2 injection into a saline aquifer containing calcite that uses this methodology.

2 ADDING CHEMICAL REACTIONS

The methodology of adding chemical reactions is based on the following:

1. We use only chemical systems that can be calculated as a function of the state variables used by CODE_BRIGHT (P_l, P_g, ϕ, T, **u**) according to thermodynamic rules for the degrees of freedom. Of course, this limits severely the number of possible chemical systems, but it is better than leaving out the chemistry completely.

2. We calculate the chemical composition of this system as a function of the state variables by means of chemical speciation codes. We used Cheproo[ii] but any other speciation code will do. Hence, also all other phase properties (density, viscosity, internal energy, etc.) can be

calculated as a function of the state variables. These functions are expressed as polynomial functions and coded in CODE_BRIGHT as constitutive and equilibrium laws.

3. We redefine the components "water", "air" and "halite" such that their mass balances represent components of the chemical system that we want to model.

Below, the methodology is illustrated by means of a H_2O–CO_2–Na–Cl–$CaCO_3$ system described by Duan and Li[iii], which may represent a saline aquifer in equilibrium with calcite. Injection of CO_2 can dissolve the calcite and increase salinity according to the following chemical reactions, all assumed to be in equilibrium:

R1: $CaCO_3(s) + H^+ = Ca^{2+} + HCO_3^-$

R2: $CO_2(aq) = CO_2(g)$

R3: $H^+ + HCO_3^- = H_2O + CO_2(aq)$

R4: $HCO_3^- = H^+ + CO_3^{2-}$

R5: $H_2O = H^+ + OH^-$

Moreover it contains Na and Cl, representing dissolved salt. The stoichiometric coefficients of this chemical system can be described by a $n_e \times n_s$ stoichiometric matrix **S** (n_e being the number of equilibrium reactions; n_s being the number of species):

$$\mathbf{S} = \begin{array}{c|cccccccccc} & H_2O & CO_2(g) & CaCO_3(s) & H^+ & Na^+ & Cl^- & Ca^{2+} & HCO_3^- & CO_2(aq) & CO_3^{2-} & OH^- \\ \hline R1 & 0 & 0 & -1 & -1 & 0 & 0 & 1 & 1 & 0 & 0 & 0 \\ R2 & 0 & 1 & 0 & 0 & 0 & 0 & 0 & 0 & -1 & 0 & 0 \\ R3 & 1 & 0 & 0 & -1 & 0 & 0 & 0 & -1 & 1 & 0 & 0 \\ R4 & 0 & 0 & 0 & 1 & 0 & 0 & 0 & -1 & 0 & 1 & 0 \\ R5 & -1 & 0 & 0 & 1 & 0 & 0 & 0 & 0 & 0 & 0 & 1 \end{array} \quad (1)$$

Furthermore we add four restrictions:

1. Isothermal conditions. A temperature of 60 ^{0}C was used, as this is the geothermal value expected both at Heletz and Hontomín CO_2 injection sites (at 1500-1600 m depth).

2. The concentration of Na^+ is constant. This of course is a bit dubious. We used a concentration of 0.4373 mol kg^{-1}, which is a typical value found in the saline aquifer of the Hontomín CO_2 injection site.

3. The same is assumed for Cl^- with the same constant concentration.

4. The liquid has zero charge, that is, the sum of the concentrations multiplied by their charge equal zero.

With these four restrictions the number of degrees of freedom reduces to one. Note that the only gaseous species is CO_2(g). Hence, the chemical composition can be calculated from one single variable, the gas pressure, which equals the partial CO_2 pressure. As a consequence, also all phase properties (densities, viscosities, etc.) are a function of only the gas pressure. We calculated the chemical composition for a series of gas pressures by means of Cheproo.

A mass balance equation can be written for every chemical component (including liquid water):

$$\sum_j U_{ij} \left(\frac{\partial c_\alpha^j}{\partial t} + \nabla \mathbf{j}_\alpha^i \right) = \sum_j U_{ij} f^j \quad i = 1, \ldots, n_s - n_e \quad (2)$$

where superscript/subscript i and j refer to components and species, subscript α refer to phases, c is concentration (in moles per volume of porous media), **j** is the advective and dispersive mass flux, f a non-chemical source/sink term and U_{ij} are elements of a component matrix, **U**, defined as the kernel matrix of the transpose of the stoichiometric matrix, $\mathbf{S}^t$, that

is, $\mathbf{U}\mathbf{S}^t = \mathbf{0}$.

One way of calculating **U** makes use of the Gauss-Jordan elimination and primary and secondary species[iv]. We chose as primary species the three species that form the major constituents of the phases (H_2O, $CO_2(g)$ and $CaCO_3(s)$) and the three remaining species in such a way that they meet the last three additional restrictions (Na^+, Cl^- and zero charge). Then the following component matrix can be deduced:

$$\mathbf{U} = \begin{array}{c|cccccccccc} & H_2O & CO_2(g) & CaCO_3(s) & H^+ & Na^+ & Cl^- & Ca^{2+} & HCO_3^- & CO_2(aq) & CO_3^{2-} & OH^- \\ \hline w & 1 & 0 & 0 & 0 & 0 & 0 & -1 & 1 & 0 & 1 & 1 \\ a & 0 & 1 & 0 & 0 & 0 & 0 & -1 & 1 & 1 & 1 & 0 \\ h & 0 & 0 & 1 & 0 & 0 & 0 & 1 & 0 & 0 & 0 & 0 \\ charge & 0 & 0 & 0 & 1 & 0 & 0 & 2 & -1 & 0 & -2 & -1 \\ Na & 0 & 0 & 0 & 0 & 1 & 0 & 0 & 0 & 0 & 0 & 0 \\ Cl & 0 & 0 & 0 & 0 & 0 & 1 & 0 & 0 & 0 & 0 & 0 \end{array} \quad (4)$$

The first three components are labeled "w", "a" and "h" because they are modeled by means of equations, that are already coded in CODE_BRIGHT. However, they have other meanings and they need to be converted to mass fractions. The concentrations of these components can be expressed as a function of the gas pressure, as explained before.

3 DEMONSTRATION EXAMPLE

We simulate CO_2 injection in a deep saline aquifer accounting for chemical reactions. We use a simple axisymmetric geometry of a 100 m thick horizontal aquifer with n injection well at the center. The top of the aquifer is situated at 1500 m depth, which corresponds to the depth of the reservoir at the Hontomin test site. The model expands laterally 5 km of the domain. The properties of the aquifer correspond to those of a permeable limestone with homogeneous grain size. The hydraulic boundary conditions are a prescribed CO_2 mass flow rate at the injection well (2.5 Mt/yr) during 1 year, a constant pressure on the outer boundary and the upper and lower boundaries are no flow boundaries. The temperature of the aquifer is 60 ºC. The mesh contains 6600 quadrilateral elements with sizes ranging from 5 m close to the injection well to 30 m close to the outer boundary.

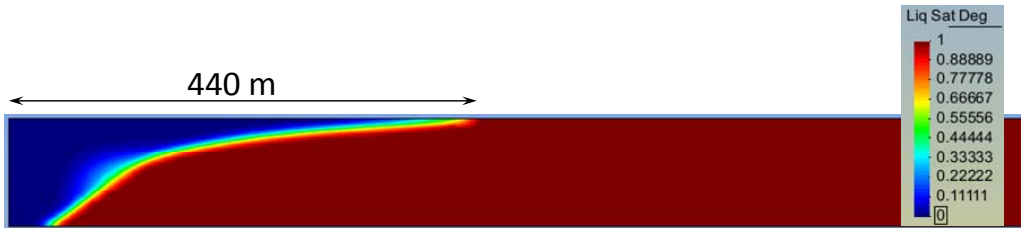

Figure 1: Liquid saturation degree after 100 days of injecting 1 Mt of CO_2.

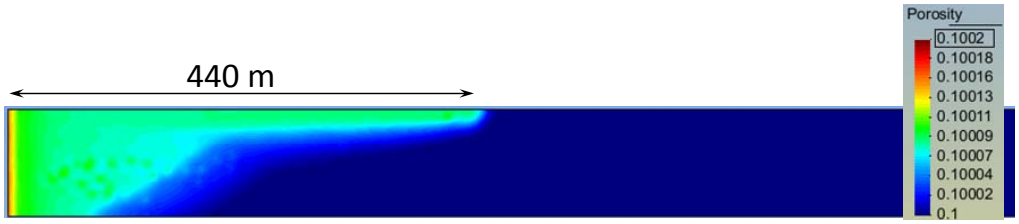

Figure 2. Porosity after 100 days of injecting 1 Mt of CO_2.

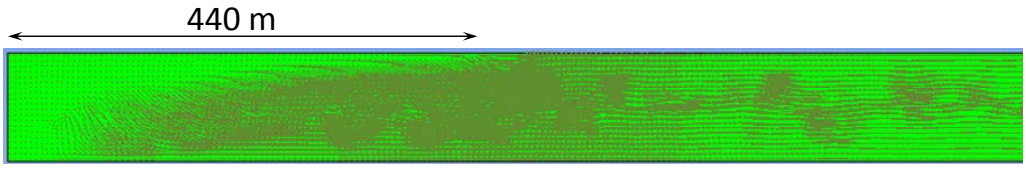

Figure 3. Water flux vectors after 100 days of injecting 1 Mt of CO2.

Figure 1 displays the CO_2 bubble after 100 days of injecting 1 Mt/yr of CO_2 and Figure 2 the porosity. CO_2 dissolution into the brine reduces the pH and dissolves calcite, which increases the porosity of the aquifer. Moreover, it increases the salinity and hence the density, causing a vertical downward flux, driven by density difference in the aqueous phase below the CO2 bubble (Figure 3).

4 SUMMARY AND CONCLUSIONS

We developed a methodology for incorporating chemical reactions into CODE_BRIGHT. Although, it is still limited to chemical systems that can be calculated as a function of the state variables used by CODE_BRIGHT (P_l, P_g, ϕ, T, **u**), it can handle more complex chemistry than the code was able to up to now (basically, halite dissolution, air dissolution and water evaporation/condensation). We added this chemistry by redefining components already existing in CODE_BRIGHT (water, air, halite, etc.) and adding new constitutive laws. The numerical solution of the resulting non-linear partial differential equations did not have to be changed. Hence, these equations are solved by means of a fully coupled Newton-Raphson approach, which is a robust method.

We applied this methodology to add chemical reactions of a H_2O-CO_2-Na-Cl-$CaCO_3$ system to CODE_BRIGHT and modeled CO_2 injection into a saline aquifer containing calcite. The model could simulate well the interaction between the development of the CO_2 bubble, dissolution of CO_2 into the brine, calcite dissolution and density dependent flow.

ACKNOWLEDGEMENT

This work was supported by the European Commission through the MUSTANG project (FP7, contract no. 227286) and by the foundation "Fundacion Ciudad de la Energia" (CIUDEN) through project ALM/09/018.

REFERENCES

[i] Olivella, S., A. Gens, J. Carrera, E.E. Alonso (1996). Numerical formulation for a simulator (CODE_BRIGHT) for the coupled analysis of saline media. Engineering Computations, 13(7), 87-112.

[ii] Bea, S.A., J. Carrera, C. Ayora, F. Batlle, M. W. Saaltink, 2009. CHEPROO: A Fortran 90 object-oriented module to solve chemical processes in Earth Science models. Computers & Geosciences, 35, 1098-1112, doi: 10.1016/j.cageo.2008.08.010.

[iii] Duan Z., D. Li (2008). Coupled phase and aqueous species equilibrium of the H2O–CO2–NaCl–CaCO3 system from 0 to 250 0C, 1 to 1000 bar with NaCl concentrations up to saturation of halite. Geochimica et Cosmochimica Acta, 72, 5128–5145, doi: 10.1016/j.gca.2008.07.025.

[iv] Steefel, C. I., K.T.B. MacQuerrie (1996). Approaches to modeling reactive transport, Reviews in Mineralogy, 34, 83-129.

IMPACT OF DRAINAGE DESIGN ON THE BEHAVIOUR OF TRANSPORT INFRASTURCTURES DUE TO ATMOSPHERIC ACTIONS

Moço-Ferreira, T.[*] and Teixeira, P. F.[*]

[*] Department of Civil Engineering, Architecture and Georesources
Instituto Superior Técnico (IST) - Technical University of Lisbon
Av. Rovisco Pais 1049-001 Lisboa, Portugal
e-mail: tmf@civil.ist.utl.pt ; pft@ist.utl.pt

Key words: Track design; drainage; bituminous subballast; unsaturated soils

Abstract. *The presence of water, along with the cyclic loading due to passing trains, has a great importance on the railroad deterioration process. Even small increases in the moisture content of trackbed layers can often result in significant reductions in the bearing capacity and stability of the composing soils contributing to a deficient deformational behavior which, in general, will affect track geometry degradation rates. In this sense, the design of an adequate drainage system maintaining low levels of moisture in the subsoil layers plays an important role in the maintenance needs of a railway track highly influenced by the condition of its infrastructure along the entire life cycle.*

The aim of this paper is to present a hydro-thermic analysis which allows assessing the impact of different drainage solutions in the performance of railway trackbeds such as the incorporation of lateral superficial drains and the use of bituminous material as subballast instead of granular layers. Rainfall, changes in the atmospheric relative humidity and temperature responsible for water infiltration/evaporation phenomena into the ground, and the consequent seasonal soil moisture variations were the main atmospheric variables considered in the analysis. The developed methodology showed its potential as a practical tool to simulate railway substructure performance under general boundary conditions and assess the impact of the adoption of different drainage solutions.

INTRODUCTION

Railway track materials and underlying soil layers are subjected to traffic loading and their mechanical behavior is highly controlled by water/moisture transfer due to atmospheric actions. Changes in water content, especially excess moisture in trackbed layers combined with traffic loads can significantly reduce railway track service life.

Integrated analyses of road pavement performance from the perspective of unsaturated soil mechanics are scarce. Some interesting results may be found in the flow (and temperature) model described by Pufahl et al.[1] and in the simulation of road pavement performance under environmental actions performed by Alonso[2].

The cyclic nature of traffic loading and atmospheric actions is related to fatigue problems in the railway infrastructure as well as an increase in the number of maintenance operations. Therefore, an efficient drainage system is crucial to maintain low levels of moisture in trackbed layers which assure an adequate mechanical behavior of these materials and reduce the deterioration rate of the overall substructure. The motivation of this paper is to assess the impact of different drainage solutions in the performance of railway trackbeds by performing a coupled hydro-thermic analysis.

NUMERICAL MODEL

The impact of different drainage solutions in the mechanical behavior of railway trackbeds is numerically assessed by using CODE_BRIGHT[3] and developing a hydro-thermic (HT) analysis. The numerical model considers daily atmospheric data concerning temperature (T), relative humidity (ρ_{vap}) and rain (Q) registered during the year of 2010 in the city of Barcelona (Figure 1a). For multiyear simulations, the annual data is simple aggregated.

The design of the railway cross section simulates a 5 meters high embankment and is based in typical geometry and layer thicknesses of ballasted high-speed lines with a granular subballast layer of 30 cm under a ballast material with a minimum of 30 cm. The subballast presents a transversal slope of 5%. The initial water content distribution corresponds to an equilibrium situation consistent with a water table located 10 m below the railway track level.

The following physical phenomena involving water transfer (Figure 1b) are considered in the HT analysis: water-flow, though the unsaturated railway trackbed layers depending on suction gradient and materials' permeability coefficient; distribution of temperature in the railway substructure; evaporation of water from the foundation soil; penetration of water through shoulders resulting from rainwater infiltration and run-off of superficial water which depends on material permeability, slope inclination and surface drainage; capillary rise from the foundation soil. The water rises from the foundation soil through the fine-grained soil up to the railway substructure (governed by suction gradients).

The railway trackbed layers are described by constitutive models and parameters which match the expected properties of materials adopted in high-speed lines construction and were detailed by Moço-Ferreira[4].

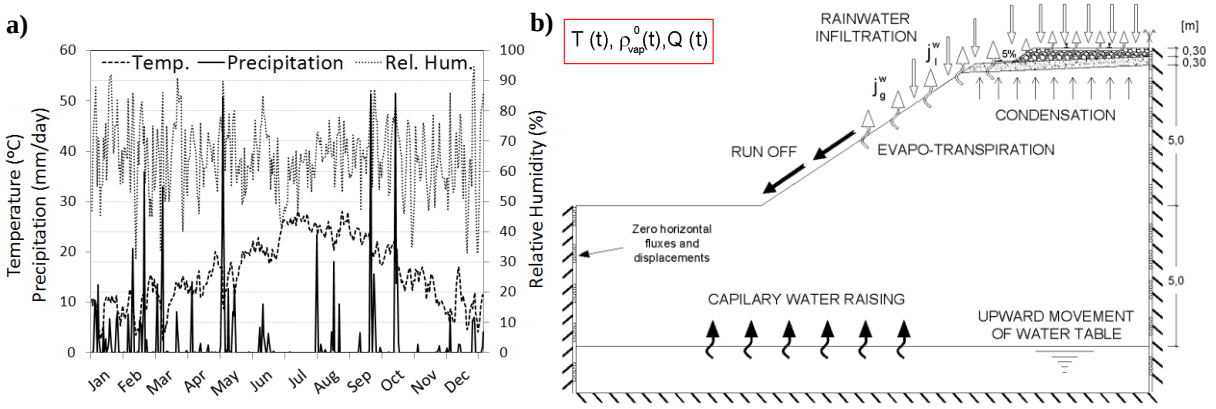

Figure 1 – a) Atmospheric data (Barcelona 2010); b) Boundary conditions.

IMPACT OF SUPERFICIAL DRAINAGE

Surface Open drains

Analysis of pavement performance concerning rainwater infiltration generally assumed that only a given percentage of the total rain intensity penetrates into the pavements layers (wide ranges from 15% to 70% are found in bibliography). In the present analysis a mechanism was developed in order to allow for surface run off and incorporation of surface drainage systems. It is considered the existence of a surface open drain in the base of the embankment slope (this drain is common to all models that will be furthered introduced). In order to assess the impact of the construction of a surface drain in the edge of the granular

subballast, the saturation degree distribution inside the railway embankment is shown in Figure 2 for 18th February when an intense rainfall was registered evidencing the difference between solutions.

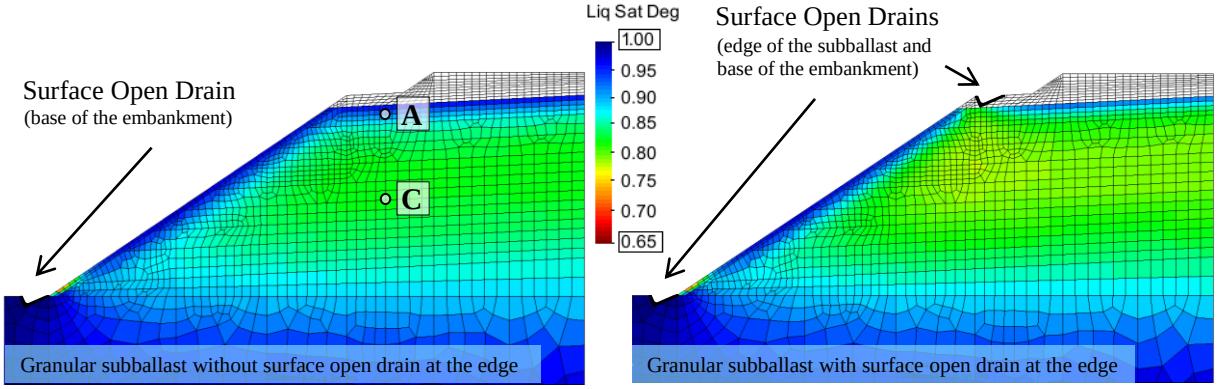

Figure 2 – Results of saturation degree for the granular subballast design: Influence of surface open drain at the edge of the subballast.

The drain collects run off water from upper layers avoiding its infiltration on the subgrade through lateral slope and maintaining lower saturation levels.

Bituminous Subballast

Unbound granular materials are usually adopted in most European railway lines. However, some innovative solutions such as the adoption of bituminous layers may bring important benefits on subgrade protection and railroad track performance, especially for the case of high-speed lines[5]. Being almost completely impervious, the use of bituminous subballast layers is expected to allow an optimal drainage of superficial rainwater while contributing to minimize fluctuations of soils moisture content[4].

The present analysis compares the performance of granular and bituminous subballast solutions. In order to reach an equivalent structural behavior between a granular subballast layer with 30 cm thickness and a bituminous one, the later must be design with 12-14 cm[5]. The results for saturation degree of both solutions (with surface open drain only at the base of the embankment) are present in Figure 3 for 18th February.

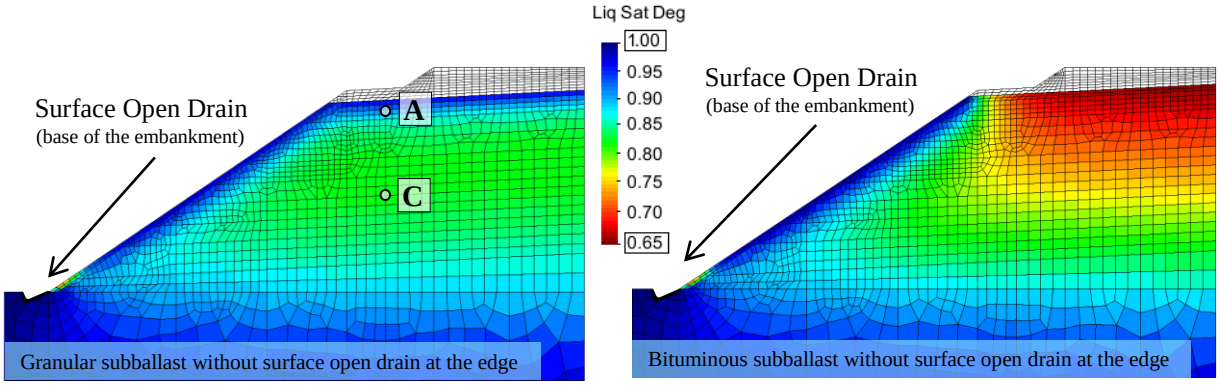

Figure 3 - Results of saturation degree for the granular and bituminous subballast solutions: Influence of bituminous protection against rainwater infiltration.

It is evident the protection conferred by the bituminous material especially in the inner points which are less exposed to the influence of lateral slope infiltration. The evolution of the saturation degree for different control points of the subgrade is also shown in Figure 4.

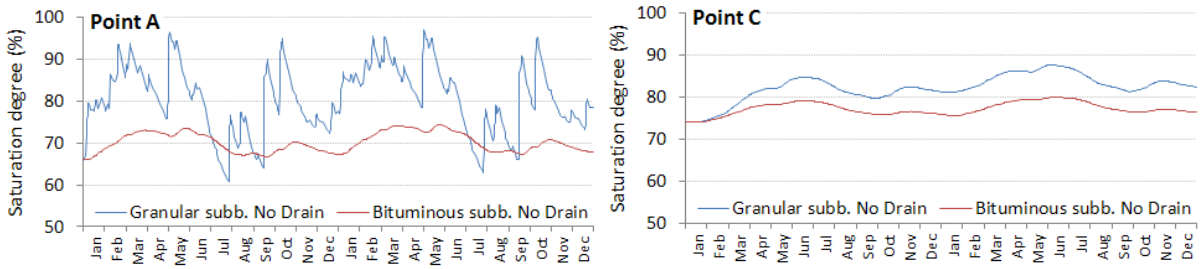

Figure 4 - Evolution of saturation degree for the granular and bituminous subballast solutions at control points (2years): Influence of bituminous protection against rainwater infiltration.

From the analysis of Figure 4 it is possible to verify that the variation of saturation degree along time associated to the bituminous solution is much smaller than the one from the granular subballast. It is worth to refer that not only variations on the saturation degree are reduced in the case of bituminous subballast but also the equilibrium moisture value inside the embankment. These results show that the design of railway tracks with an impermeable bituminous layer may have a significant impact on the overall behavior of the substructure.

CONCLUSIONS

The described hydro-thermic analysis presents a suitable methodology to assess the impact of different drainage solutions in the behavior of railway trackbed layers exposed to general atmospheric actions. In the case of lines constructed over embankments, the presented results showed that surface open drains and, in particular, bituminous subballast layers are effective in protecting trackbed layers from atmospheric actions and maintaining low levels of moisture along time.

REFERENCES

[1] Pufahl, D. E., R. L. Lytton and H. S. Liang (1990). "Integrated computer model to estimate moisture and temperature effects beneath pavements". *Transportation Research Record*, No 1286, Washington D.C., pp. 259-269.

[2] Alonso, E. E. (1998). "Suction and moisture regimes in roadway bases and subgrades". *Simposio Internacional: Drenaje Interno de Firmes y Explanadas*, Granada, pp. 57-104.

[3] Olivella, S., Gens, A., Carrera, J. and Alonso, E. E. (1996). "Numerical formulation for simulator (CODE_BRIGHT) for coupled analysis of saline media". *Engineering computations*, Vol. 13, No 7, pp. 87-112.

[4] Moço-Ferreira, T., Teixeira, P. F. and Cardoso, R. (2011). "Impact of bituminous subballast on railroad track deformation considering atmospheric actions", *Journal of Geotechnical and Geoenvironmental Engineering*, Vol. 137, No 3, DOI: 10.1061/(ASCE)GT.1943-5606.0000435.

[5] Teixeira, P. F., A. López Pita, C. Casas, A. Bachiller and F. Robusté (2006). "Improvements in high-speed ballasted track design: benefits of bituminous subballast layers". Transportation Research Record: Journal of the Transportation Research Board, No 1943, pp.43-49.

THERMO-HYDRO-MECHANICAL SIMULATION OF GEOTHERMAL RESERVOIR STIMULATION

Silvia De Simone[*†], Victor Vilarrasa[*†], Jesús Carrera[*], Andrés Alcolea[§] & Peter Meier[§]

[*] GHS, Institute of Environmental Assessment and Water Research (IDAEA),
Consejo Superior de Investigaciones Científicas (CSIC)
Jordi Girona 18-26, 08034 Barcelona, Spain
e-mail: silviadesi@gmail.com

† GHS, Department of Geotechnical Engineering and Geosciences,
Technical University of Catalonia (UPC-BarcelonaTech),
Jordi Girona 1-3, 08034 Barcelona, Spain

§ Geo-Energie Suisse AG, Steinentorberg 26, CH-4051 Basel, Switzerland

Key words: geothermal reservoirs, THM coupling, induced seismicity.

Abstract. *In general terms, induced seismicity occurs when the isotropically effective stress reduction, due to the fluid pressure increase caused by fluid injection, is high enough to produce failure conditions. The objective of the simulation is to test the conjecture that cold water injection produces mechanical instability not only due to hydraulic effects, but also due to coupled thermal effects. Hydro mechanical (HM) and thermo hydro mechanical (THM) numerical simulations have been performed on a very simplified geometry of a horizontal fracture in order to analyze the processes involved in geothermal reservoir stimulation. The results confirm that indeed THM effective stresses are consistently more unstable (closer to a hypothetical yield surface) than HM effective stresses.*

1 INTRODUCTION

Deep hot rocks represent a source of renewable energy. Geothermal energy production can be simply achieved by drilling two wells into a hot deep rock, injecting cold water into one of them and recovering hot water/steam from the other one. This enables to produce electricity and/or heat.

To improve the economic efficiency of the heat exchange, high permeability rock is necessary. Generally, naturally fractured hot rocks are intercepted by the wells and their permeability is improved by hydraulic stimulation, obtaining "Enhanced Geothermal Systems" (EGS). In fact, water injection produces overpressure that reduces the effective stresses. If failure conditions are reached, slip occurs, leading to fracture opening due to dilatancy. These processes trigger microseismic events, that should end when injection stop. Nevertheless, it has been observed that microseismic events are still induced once injection is stopped. Parotidis *et al.*[1] assumed that pore-pressure diffusion is the main triggering mechanism for these post-injection events. However, the fact that the largest seismic events can occur after the end of injection, like occurred in Basel (Switzerland)[2], cannot be explained by pressure diffusion alone, because its magnitude decreases with time.

Actually, both at Basel and Soultz[3], the injected water was cold. The temperature contrast between the reservoir (190 ºC at 5000 m deep)[4] and the injected water (at atmospheric conditions at surface) was large. This produces an additional reduction in effective stresses due to thermal strain[5,6] that enhances the seismic potential. Hence, coupled thermo-hydro-mechanical analyses are needed to fully understand the processes involved in geothermal reservoir stimulation.

To study the effect of the cooling front caused by cold water injection on thermoelastic strain, coupled hydro-mechanical (HM) and thermo-hydro-mechanical (THM) numerical simulations are performed, simulating water injection into a simplified geometry.

2 PROBLEM SET-UP

The geometry taken into account considers a horizontal 1 m-thick fractured zone underlain and overlaid by a 250 m-thick low-permeability matrix. The model extends laterally 2000 m and is axisymmetric around the vertical well axis, simulating a 2D vertical section of the formation. The top of the fracture filling is located at a depth of 4250 m.

The fracture filling is considered like a continuous porous medium, with intrinsic permeability k=10^{-13} m^2 and porosity ϕ=0.5; the low permeability matrix has intrinsic permeability k=10^{-18} m^2 and porosity ϕ=0.01. A linear elastic constitutive model is assumed with a Young's modulus of E=100 MPa for the fracture filling and of E=10000 MPa for the matrix. Poisson's ratio is assumed to be ν=0.3 for both materials.

Initial conditions correspond to hydrostatic pressure, uniform temperature gradient and lithostatic normal stress. The stress regime is considered axisymmetric and the vertical stress is assumed greater than the horizontal stress with $\sigma'_h = 0.75\sigma'_v$.

A constant pressure boundary condition of 40 MPa, which corresponds to the hydrostatic pressure at the top of the model, is imposed at the top of the outer boundary. An overburden equal to 92 MPa, which corresponds to the lithostatic vertical stress, is imposed at the upper boundary. A mechanical condition of no displacement perpendicular to the boundary is imposed in the other boundaries. The injection flow rate is of 3 kg/s and is uniformly distributed along the contact between the well, with a radius of 0.5 m, and the fracture filling. Water injection lasts for 10 days.

Additionally, thermal conditions are imposed for the thermo-hydro-mechanical model: a temperature of 140 ºC is imposed at the top of the outer boundary, which corresponds to a surface temperature of 5 ºC and a geothermal gradient of 34 ºC/km. Water is injected at 60 ºC, which is a much lower temperature than that of the fracture.

A structured mesh with 8925 quadrilateral elements is used. The mesh is refined close to the injection well, in the fracture filling and close to it. Simulations are performed using the finite element numerical code CODE_BRIGHT[7,8].

3 RESULTS

Water injection in a porous or fractured medium produces an overpressure that reduces the effective stresses, which tends to open the fracture. Furthermore, if water is injected colder than the formation, the decrease in temperature causes two additional hydro-mechanical effects: increase in fluid viscosity and thermal contraction. The temperature increase in liquid

viscosity causes a decrease in hydraulic conductivity. Thus, injection of cold water produces a larger overpressure than injection of warm water.

In the THM simulation, the cooling front propagates within the first 20 m of the fracture in the longitudinal direction and penetrates 1 m in the matrix in the transverse direction after 10 days of cold water injection. Thus, two slopes can be observed when plotting pressure as a function of distance from the well (Fig. 1): in the first 20 meters, affected by the cold front, the pressure curve displays a greater slope than in the rest of the fractured zone affected by fluid injection.

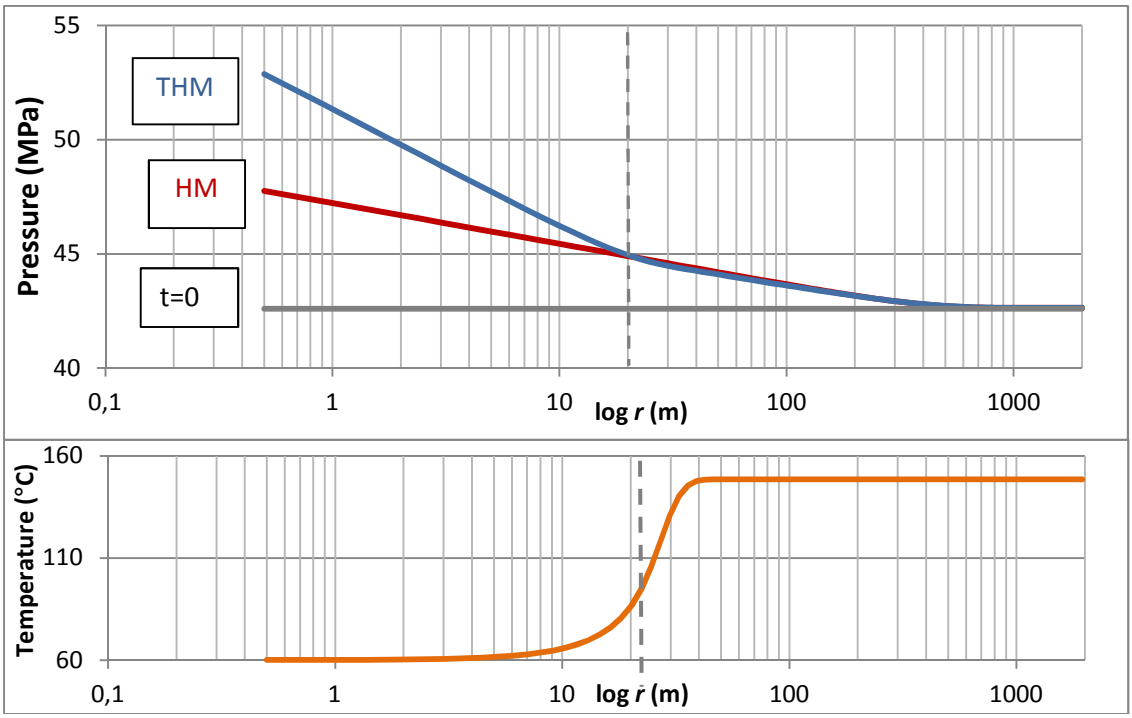

Figure 1. Pressure and temperature inside the fracture filling vs distance from the injection well after 10 days of injection.

Regarding stresses and strains, the cooling front causes thermal contractions of the rock. The effect of this contraction is non-trivial. While the contraction of the fracture filling tends to close it (competing against the expansion caused by overpressure), the contraction of the matrix that is cooled tends to open the fractured zone. The magnitude of the thermal effect is proportional to the temperature drop and to the rock stiffness.

In the studied case, with a fracture filling having E=100 MPa, the thermal contraction of the fracture filling partly compensates the additional expansion caused by the greater overpressure. As a result, inside the fracture, stability is comparable to that of the isothermal case (Table1). Fractured zone expansion causes mechanical contraction of the matrix. Furthermore the matrix affected by the temperature decrease undergoes an additional contraction, opening the fractured zone even more (Fig. 2).

This behavior results in a significant reduction of the stability at the fracture-matrix contact when accounting for cold water injection (Table 1).

Table 1: Mobilized friction angle after 10 days of injection of water in thermal equilibrium with the fracture (HM) and cold water (THM).

Mobilized friction angle	HM	THM
fracture-matrix contact	8.0	11.7
inside fracture	7.9	7.8

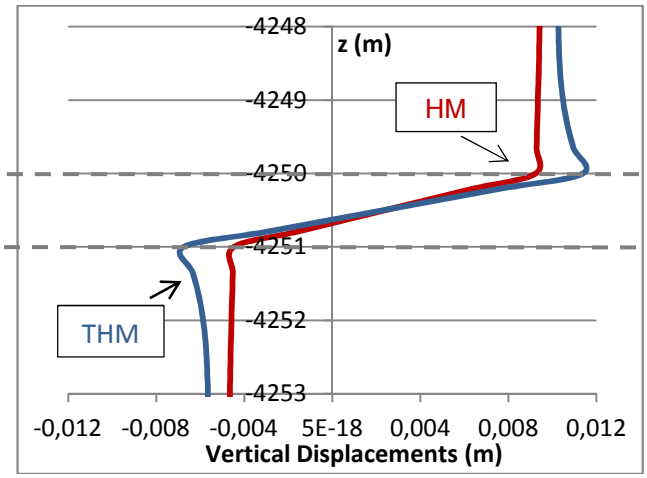

Figure 2: Vertical displacements vs depth for a section placed 3 m away from the injection well - detail of the 2 m above and below the fractured zone (placed between the dashed lines).

4 CONCLUSIONS

The numerical simulations show the influence of thermal effects in the processes of deformation involved in the geothermal hydraulic stimulations. Cold water injection produces a higher overpressure than warm water injection. Thus, a greater effective stress reduction and a larger fracture opening tendency occur. However, cold temperature causes thermal strains of the rock: contraction of the fracture filling tends to compensate hydraulic expansion; but cooling of the matrix close to the fracture acts opening the fracture. These opposing trends lead to more unstable conditions at the fracture edges. Therefore, induced seismicity is likely to be triggered when injecting cold water.

REFERENCES

[1] Parotidis M., Shapiro S.A. & Rothert E. (2004). Back front of seismicity induced after termination of borehole fluid injection. Geophysical Research Letters, 31, L02612, doi:10.1029/2003GL018987.

[2] Ripperger J., Kästli P., Fäh D. & Giardini D. (2009). Ground motion and macroseismic intensities of a seismic event related to geothermal reservoir stimulation below the city of Basel – observations and modeling. Geophysics Journal International, 179:1757-1771.

[3] Evans K.F., Moriya H., Niitsuma H., Jones R. H., Phillips W. S., Genter A., Sausse J., Jung R., Baria R. (2005). Microseismicity and permeability enhancement of hydrogeologic structures during massive fluid injections into granite at 3 km depth at the Soultz HDR site. Geoph. Journal International, 160: 388-412.

[4] Häring M.O., Schanz U., Ladner F. & Dyer B.C. (2008). Characterization of the Basel 1 enhanced geothermal system. Geothermics, 37:469-495.

[5] Segall P. & Fitzgerald S.D. (1998). A note on induced stress changes in hydrocarbon and geothermal reservoirs. Tectonophysics, 289:117-128.

[6] Ghassemi A., Tarasovs S. & Cheng A.H.-D. (2007). A 3-D study of the effects of thermomechanical loads on fracture slip in enhanced geothermal reservoirs. International Journal of Rock Mechanics and Mining Sciences, 44:1132-1148.

[7] Olivella S., Carrera J., Gens A., Alonso E. E. (1994). Non-isothermal Multiphase Flow of Brine and Gas through Saline media. Transport in Porous Media, 15, 271:293

[8] Olivella S., Gens A., Carrera J., Alonso E. E. (1996). Numerical Formulation for a Simulator (CODE_BRIGHT) for the Coupled Analysis of Saline Media. Engineering Computations, Vol 13 (7): 87-112.

GRS RESEARCH PROGRAMME

DEVELOPMENT AND IMPLEMENTATION OF CONSTITUTIVE MODELS FOR DAMAGE AND SEALING OF CLAY ROCK

Chun-Liang ZHANG and Oliver Czaikowski
Gesellschaft für Anlagen- und Reaktorsicherheit (GRS), D-38122 Braunschweig, Germany
e-mail: chun-liang.zhang@grs.de, web page: http://www.grs.de/

1 INTRODUCTION

With regard to the new German approach of the safe containment of radioactive waste in an isolating rock zone (IRZ) (instead of considering release scenarios as has been done preferentially in the past), it is of paramount importance to confirm constitutive models enabling adequate prediction of the long-term processes prevailing in the host rock, particularly the recovery of the excavation damaged zone (EDZ) around the repository openings. The computer code CODE_BRIGHT developed by UPC has been used by GRS since 10 years for the analysis of coupled thermo-hydro-mechanical processes in clay host rock (and also in rock salt). Recently, in the framework of the EC project TIMODAZ, GRS has performed a series of benchmark modelling exercises to validate the capabilities of the constitutive models implemented in the code for description of the EDZ development in clay host rock. Our own results and the results from the other partners using different models and codes suggest that an enhancement of the models in terms of their predictive capability is needed, especially with regard to the following aspects:

- mechanical damage evolution and induced permeability changes
- self-sealing of EDZ due to re-compaction and re-saturation
- time dependence of rock deformation and EDZ recovery
- swelling behaviour in different confining conditions
- thermal effects on the sealing of EDZ
- anisotropy of the THM behaviour

In order to improve and develop advanced constitutive models for description of the damage and sealing of clay rock, a research programme has been launched by GRS. It will be conducted from May 2011 to June 2015. This project is funded by the German Federal Ministry of Economics and Technology (BMWi). This programme will be supported by ANDRA and UPC/CIMNE. As the code developer, UPC/CIMNE is asked to review and to consult the model development work and implement the advanced models in CODE_BRIGHT within the frame of the consortium agreement. ANDRA will provide core samples from the URL Bure for laboratory experiments and relevant in-situ measurements for model validation.

2 OBJECTIVES

The goal of the project is the development of advanced constitutive models for description of damage and sealing of clay rock with the following specific objectives:

- Establishment of a database from laboratory experiments for
  - o understanding of the damage and sealing mechanisms
  - o formulation of constitutive equations
  - o determination of model parameters
  - o validation of the advanced models
- Model development and improvement focusing on

- damage evolution with stress
- damage-induced permeability changes
- stress-compaction-permeability relationships for fractured clay rock
- time dependence of rock deformation and fracture compaction
- water flow effects on sealing of fractures

- Implementation of the advanced models in CODE_BRIGHT
- Validation of the advanced models by simulation of lab and in-situ experiments and comparison with the observations

3 WORK PROGRAMME

Corresponding to the objectives mentioned above, the project will be conducted within the work packages defined as below. The work programme will be performed in steps and the progress will be reviewed regularly. Depending on the progress, it may become necessary to shift the later steps to a second phase.

3.1 Review of available data

A database with high quality is necessary for the development of constitutive models. In the past, GRS carried out comprehensive laboratory experiments on the Callovo-Oxfordian argillite (COX) and produced a great amount of data. GRS' data and other interesting results will be reviewed, summarized, and appraised. A possible lack of data for the model development will be compensated by further laboratory tests to be conducted within this project.

3.2 Laboratory experiments

Based on our current knowledge, specific laboratory experiments are necessary to be carried out for the model development. The COX clay rock is used as testing material.

Damage / re-compaction tests

Considering the conditions of the EDZ development around underground openings, a series of combined damage and re-compaction tests will be performed on COX samples in triaxial apparatus. Each sample will be loaded in three stages: 1) isotropic compaction up to the in-situ overburden stress, 2) deviatoric stressing by increasing axial stress at reduced lateral confining stress up to failure, and 3) re-compaction by increasing the confining stress. During the tests, axial / radial / volumetric strains, gas permeability and ultrasonic wave velocity in the axial load direction will be recorded. The following results can be expected:

- Stress-strain behaviour and parameters until post-failure (residual strength)
- Damage evolution with stress detected by stiffness and wave velocity changes
- Permeability change in relation with strain or damage parameters
- Re-compaction behaviour of fractured samples
- Permeability reduction as function of the re-compaction

Long-term creep tests

The long-term deformation behaviour of the clay host rock is one of the most important factors governing the sealing of fractures in the EDZ. Triaxial creep tests will be carried out on COX samples under multiple load conditions. In order to achieve the original rock state, the samples will be pre-consolidated under the in-situ isostatic stress. Following that, deviatoric stress states will be adjusted to different levels covering the stress state in the EDZ. Each creep phase shall reach a quasi-steady state. Damage effect on the strain rate shall be

determined. Based on the creep data, the time-dependent deformation behaviour will be derived in terms of strain rate as function of applied stress.

Fracture sealing tests

The sealing behaviour of fractures will be determined by compression of artificially fractured samples under various confining stresses. During the compaction, permeability changes will be measured by flowing nitrogen gas or synthetic pore water through the fractured samples. From the data, fracture closure in relation to confining stress and the corresponding permeability can be obtained. Comparison of permeability values determined by gas and water flow will highlight effects of moisture-induced swelling/slaking on the fracture sealing.

Swelling tests

There is still a debate about the conceptual model or stress concept for highly-consolidated clay rocks like the Callovo-Oxfordian argillite. Up to now, the clay rocks are generally treated as the conventional porous medium, by assuming that contacts between neighbouring particles are solid to solid and the interparticle contact pressure is equivalent to the effective stress in the material. Recently, GRS has provided experimental evidence that the great portion of the water content in the COX clay rock are adsorbed on mineral surfaces and capable of bearing external loads and even carrying the lithostatic stress like solid particles. The disjoining (swelling) pressure acting in the interparticle water-films is equivalent to the effective stress. This fundamental issue will be examined by conducting some specially designed swelling tests on COX samples under various constrained conditions.

3.3 Model development

CODE_BRIGHT is used by GRS for the analysis of THM processes in clay host rock and clay-based barriers in repositories. There are various constitutive models implemented in the code for different materials and different types of THM behaviour. The application results suggest that the complex THM phenomena observed in many laboratory and field experiments can be reasonably represented by the numerical calculations with use of adequate models and parameters.

Recently, UPC has developed and implemented a damage-elastoplastic model for argillaceous rock, which has been applied by GRS for modelling laboratory tests and in-situ experiments within several projects (NFPRO, TIMODAZ, etc.). Many important features of the short-term behaviour can be captured by the model. However, it still needs to be improved and advanced in regard to the following aspects dealing with damage and sealing of clay rock:

1. damage evolution and induced permeability changes
2. re-compaction and permeability changes of damaged rock
3. time dependence of deformation and compaction
4. water flow effects on sealing of fractures

The model development is planned to be done by GRS with the consultation support of UPC. The model development will be carried out step by step.

3.4 Model implementation and validation

The advanced models are foreseen to be implemented in CODE_BRIGHT by CIMNE within the frame of the consortium agreement. The developed models and their implementation will be validated by UPC/CIMNE and GRS together. The model validation will be performed by simulation of specially designed laboratory tests and in-situ experiments performed in the URL Bure (to be identified by ANDRA, GRS and UPC/CIMNE).

THM MODELLING OF FINAL DISPOSAL REPOSITORY INCLUIDING GAP ELEMENT

Erdem Toprak[1], Sebastia Olivella[1], Nadia Mokni[1], Xavier Pintado[2]

[1] Escola de Camins, UPC, Barcelona, Spain
[2] B+TECH, Helsinki, Finland

This paper presents preliminary analyses of coupled Thermo-Hydro-Mechanical (THM) processes in the future nuclear waste repository in Olkiluoto (www.posiva.fi). A finite element program Code_Bright is used to perform modeling calculations of disposal tunnels in an underground repository for spent nuclear fuel.

The repository will consist of a series of deposition holes in the bedrock. Bentonite buffer rings will surround the copper canisters containing spent fuel. As a protecting and isolating barrier between the waste canisters and the surrounding host rock, MX80 bentonite will be used as buffer material. Friedland clay is considered one of the best candidates to be used as drift backfill material to meet the long-term performance requirements set for backfilling of a disposal tunnel in the repository. Figure 1 shows a cross section of the spent nuclear final disposal facility.

The time required for reaching full saturation, maximum temperature reached in canister, deformations in the buffer-backfill interface and stress-deformation balance in this interaction and also modeling of gap between canister and buffer ring are the main issued addressed of this study.

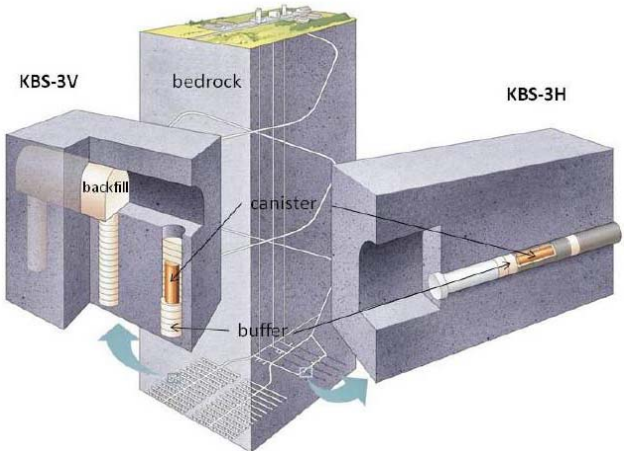

Figure 1. *Alternative realizations of the KBS-3 spent fuel disposal method (In this study, it has been modeled the vertical deposition hole)*

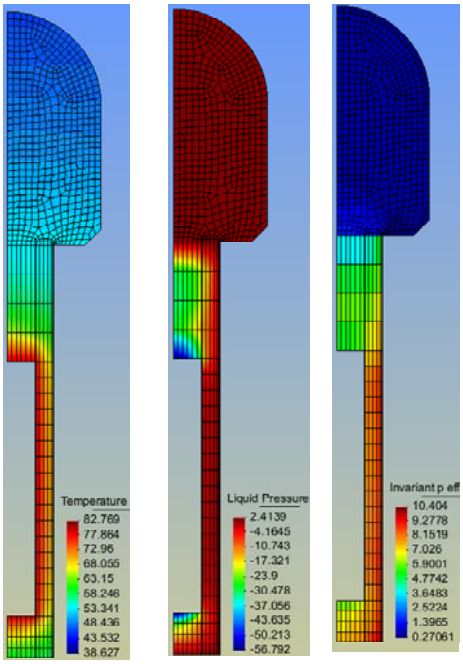

Figure 2. *Evolution of temperature (30 years), liquid pressure (3 years) and mean effective stress (10 years)*

A fundamental issue in modeling was to determine relevant thermal boundary conditions so that the details of THM-behavior could be captured by defining proper near-field thermal boundaries. In this study, it has been shown that temperature on the considered close boundaries depends on initial canister power, fuel power decay characteristic and rock thermal properties. The thermal boundary conditions fixed at the

THM modeling have been calculated solving the thermal problem for the entire repository with the analytical solution (Ikonen, 2005).

With regard to the hydraulic analyses, the time required for full saturation is sensitive to vapor diffusion, hydraulic conductivity and water retention curve of the buffer and the hydraulic conductivity of the rock. A sensitivity study has been performed to investigate the base case performance and its correspondence with realistic conditions.

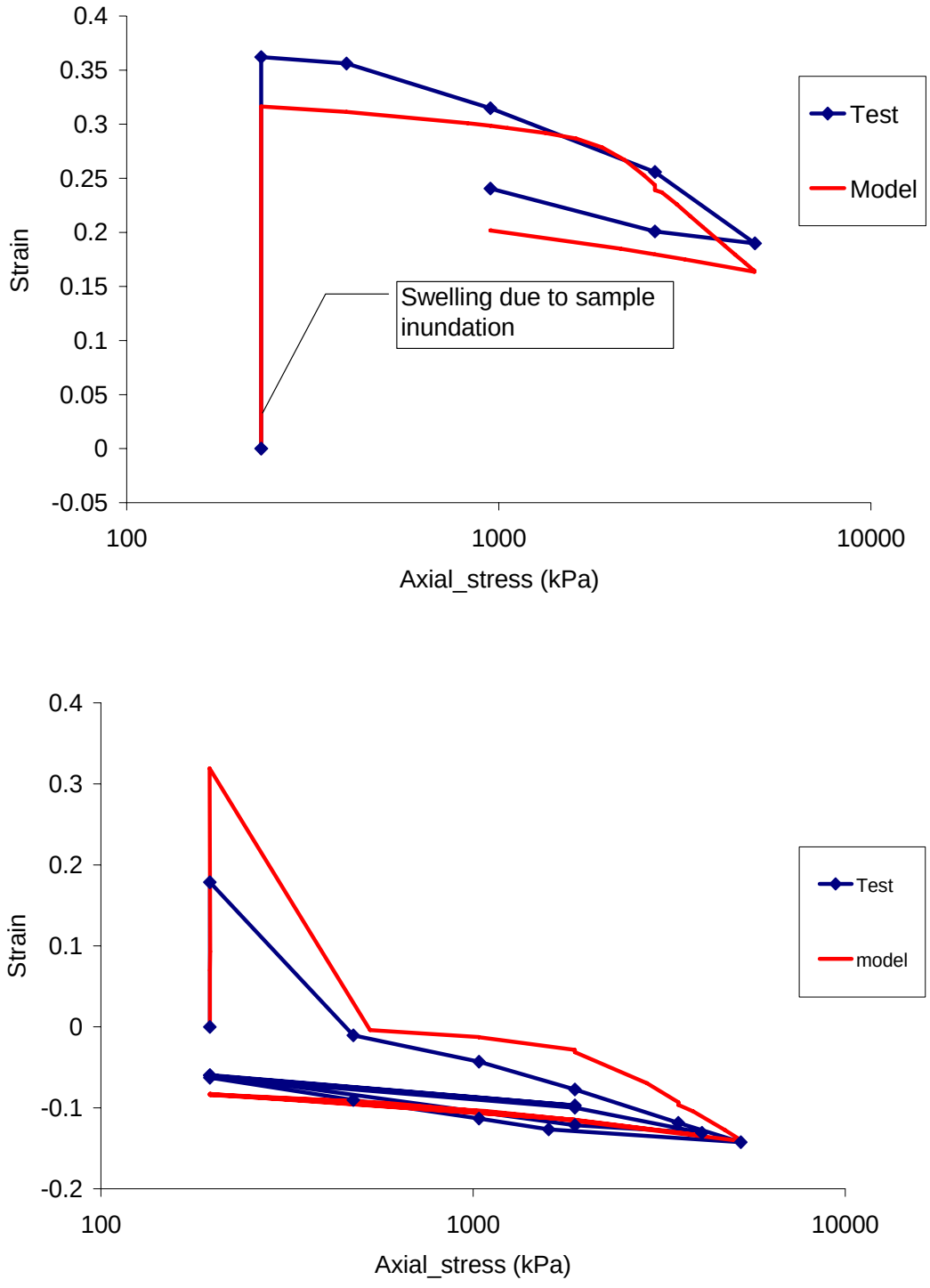

Figure 3. *Modeling and experimental results of oedemeter tests*

The modeling process of buffer-backfill interface is an important part of tunnel backfill design. The calculations will aim to find out deformations in this intersection whose behavior is important for the buffer swelling. In order to investigate the hydro-mechanical behavior of MX80 bentonite which is the buffer material, a series of laboratory tests have been started up by POSIVA and carried out at B+TECH laboratory. Two types of tests have been performed: oedometer tests and infiltration tests. These tests have been modeled using the finite element code Code_Bright for model calibrations. The Barcelona Basic Model (BBM) (Alonso et al., 1990) has been used to model the mechanical behavior of the material.

Figures 3 display the vertical stress-strain relationship of calibrated oedometer tests. The plots show comparisons between the experimental data and the numerical simulations. For both tests, the modeled results fit quite well with the experimental data. The model predicts well the swelling deformations that occur during the wetting phase. The calculated swelling deformations for the tests are in the same order of magnitude as the measured value.

There is an air-filled gap between canister and the buffer ring according to reference design. In its unsaturated state, buffer will not transfer heat efficiently that may disturb the heat dissipation and lead to higher canister temperature. Therefore gap modeling was an essential part of this study. Heat transfer across the air-filled gap occurs by conduction, radiation and convection. An equivalent conductivity combining effect of conduction and radiation is considered. Figure 4 and 5 show evolution of some relevant variables such as temperature, liquid pressure and mean effective stresses. The effect of gap is clearly seen via these figures, for example because the temperature at both sides of the gap is different but collapses to the same value as the gap closes (before 10 years).

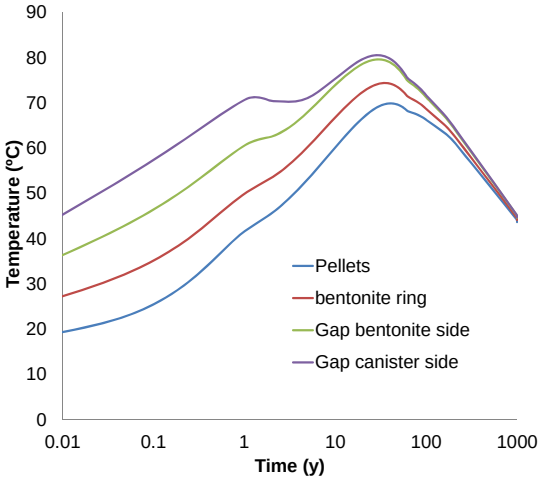

Figure 4. *Temperature evolution of materials*

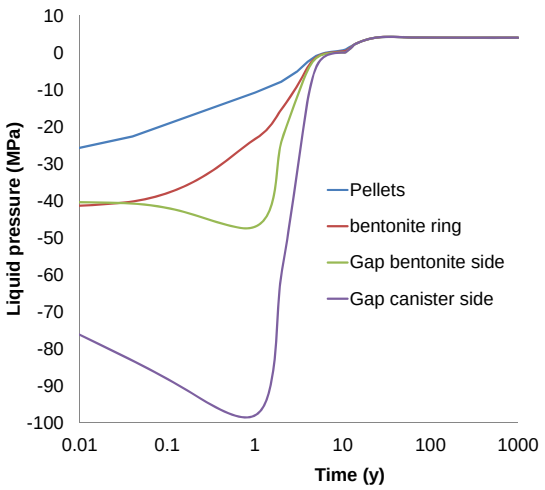

Figure 5. *Liquid pressure evolution of materials*

It should be noted that this study includes some assumptions and simplifications (such as 2D axisymmetric modeling). There are several alternatives for the materials (buffer, backfill and pellets) that are going to be considered in the repository. Therefore, some parameters of these materials should keep handling through sensitivity analyses as a future work.

References

Alonso E.E., Gens A and Josa A, 1990.”A constitutive model for partially saturated soils”. Géotechnique, 40(3): 405-430

Hokmark. H. 2003. Hydration of the bentonite buffer in a KBS-3 repository. Applied Clay Science 26 (2004) 219 - 233

Ikonen, K. 2003. Thermal Analyses of Spent Nuclear Fuel Repository

Toprak Erdem, Mokni Nadia, Olivella Sebastia, 2011. THM Modelling of Onkalo Project Preliminary Modelling Study.

CHEMO-HYDRO-MECHANICAL MODELLING OF IN-SITU DISPOSAL OF A BITUMINIZED RADIOACTIVE WASTE IN BOOM CLAY

N. Mokni[1], S. Olivella[1], E. Valcke[2],A. Mariën[2], S. Smets[2], X. Li[3], X.Sillen[4]

1. Department of Geotechnical Engineering and Geosciences, Universitat Politècnica de Catalunya, Barcelona, Spain (nadia.mokni@upc.edu)

2. Waste and Disposal Expert Group, The Belgian Nuclear Research Centre (SCK•CEN), Boeretang 200, 2400 Mol, Belgium

3. EIG EURIDICE, Boeretang 200, 2400 Mol, Belgium

4. ONDRAF/NIRAS, Kunstlaan 14,1210 Brussel,Belgium

Key words: CHM coupled analysis, Boom Clay, in-situ disposal

Abstract. *In this paper, the impact of osmotic forces on the swelling of porous materials containing salts is investigated. The problem is complex as solutes affect the swelling of the material in different ways. A CHM formulation is discussed. The equations include the effect of coupled transport phenomena mainly the osmotic flux. The CHM coupled formulation is used to model the in-situ disposal of bitumunized radioactive waste in Boom Clay.*

1 INTRODUCTION

The current reference solution of the Belgian Agency for the Management of Radioactive Waste and Fissile Materials (ONDRAF/NIRAS) envisages underground disposal of Eurobitum Bituminized radioactive Waste (BW) in a geologically stable clay formation [1]. In Belgium, the Boom Clay, which is a 30 to 35 million years old and ~100 m thick marine sediment is being studied as a potential host formation because of its favorable properties to limit and delay the migration of the leached radionuclides to the biosphere over extended periods of time. The current disposal concept foresees that several drums (220 litres) of Eurobitum would be grouped in thick-walled cement-based secondary containers, which in turn would be placed in concrete-lined disposal galleries that are excavated at mid-depth in the clay layer. Only 80-90 % of the total volume of the drum is filled with Eurobitum .The remaining voids between the containers would be backfilled with a cement-based material. The interaction between the BW and the host clay formation is a very complicated chemo-hydro-mechanical process and depends not only on the hydro-mechanical behaviour of the Boom Clay itself, but also on that of the BW. In fact, the osmosis-induced uptake of water by the dehydrated hygroscopic salts embedded in the waste induces a geo-mechanical perturbation of the host formation, caused by the swelling and the increase of the pressure in and around the waste.

The objectives of the Chemo-Hydro-Chemical (CHM) analysis presented in this work are (i) to get insights on the kinetics of water uptake by BW, dissolution of the embedded $NaNO_3$ crystals, solute leaching, and maximum generated pressure under disposal conditions and (ii) to study the stress redistribution due to the recompression of the clay around a gallery caused by the swelling pressure of the bitumen and the admissible swelling pressure for Boom clay.

2 COUPLED CHM FORMULATION

A CHM formulation of chemically and hydraulically coupled flow processes in porous materials containing salt crystals is discussed. The formulation incorporates the strong dependence of the efficiency of the membrane on porosity and assumes the existence of high concentration gradients that are maintained for a long time and that influences the density and motion of the fluid.

The constitutive equations that relate the mass-average flow of fluid and the mass flow of solute to chemical and pressure gradients are as follows [2]:

(i) Flux of liquid phase induced by both pressure and concentration gradients

$$\mathbf{J}_l = -\frac{\mathbf{k}k_{rl}}{\mu}\left(\nabla p + \rho_l \mathbf{g}\nabla z\right) + \frac{\alpha_s}{\mu}\mathbf{k}\sigma\nabla(w_l^s); \quad \alpha_s = \frac{k_{rl}RT\rho_l}{M_s} \tag{1}$$

This is an advective flux in the sense that it drags both the solute and the water.

(ii) Non-advective flux of solute:

$$\mathbf{J}_l^s = -\sigma w_l^s \rho_l \mathbf{J}_l - D\rho_l(1-\sigma)(1+\gamma w_l^s)\nabla w_l^s \; ; \tag{2}$$

$$\gamma = \frac{1}{\rho_l}\frac{\partial \rho_l}{\partial w_l^s}$$

(iii) Non-advective flux of water including ultrafiltration is written as:

$$\mathbf{J}_l^w = \frac{\beta}{\alpha}\sigma w_l^s \rho_l \mathbf{J}_l - D\rho_l(1-\sigma)(1-\gamma w_l^w)\nabla w_l^w \tag{3}$$

$$\alpha = 1 + \frac{1}{\rho_l}\frac{\partial \rho_l}{\partial w_l^s} w_l^s = 1 + \gamma w_l^s \qquad \beta = 1 + \frac{1}{\rho_l}\frac{\partial \rho_l}{\partial w_l^w} w_l^w = 1 - \gamma w_l^w$$

Where $\mathbf{k}$ [m^2] denotes the intrinsic permeability tensor, k_{rl} [-] denotes the relative permeability of the liquid, $\mathbf{g}$ is the gravity vector, μ [MPa s] is the dynamic viscosity, p [MPa] is the hydraulic pressure, w_l^s is the mass fraction of solute in the liquid phase, w_l^w is the mass fraction of water in the liquid phase, R [J/(mol K)] is the gas constant, T [K] is the temperature, ρ_l [kg/m^3] is the liquid density, M_s [kg/mol] is the solute molar mass, σ [-] is the efficiency coefficient and D [m^2/s] is the diffusion coefficient.

The coupled migration of dissolved salt and water is controlled by the following variables:

(i) The intrinsic permeability k (m^2), which controls the flow of water due to hydraulic and osmotic pressure gradients. It also controls the flow of solutes by advection. The intrinsic permeability is assumed to be dependent on porosity.

(ii) The osmotic efficiency σ, which controls the flow of water and solutes due to osmotic effects. This parameter describes the non-ideality of a membrane behavior. It ranges from 1 for an ideal membrane to 0 for porous media having no membrane properties.

It is postulated that the efficiency coefficient is a nonlinear function of the porosity. It has to be noticed that Equations 2 and 3 fall into Darcy and Fick laws, respectively, when osmotic effects are not present, i.e. when σ=0.

(iii) The diffusivity of solutes and water (m^2/s), which control the diffusion of dissolved salt and water. The parameter D is considered as an effective diffusion coefficient equal to $D = \tau\phi_f D_0$ where τ is the tortuosity and D_0 is a Fickian diffusion coefficient for a solute in free water.

The effective diffusivity for semi-permeable membranes is defined as $D^* = (1-\sigma)D$. Therefore, for media presenting ideal membrane properties the diffusion of the solute and water is completely prohibited.

To establish the balance equations, the compositional approach is adopted consisting in balancing the species (solid matrix, salt as crystal or dissolved salt, water as liquid or evaporated in the gas phase, and air as gas or dissolved in the liquid phase) rather than the phases (solid: bituminous matrix and crystals, liquid and gas). The mass balance equations for water, dissolved salts, crystals and solid phase, including the coupled flows, namely osmotic flow and ultrafiltration, and the dissolution/precipitation of salts, are detailed in [2]. The formulation has been included in CODE_BRIGHT [3].

The CHM formulation was used to analyse the influence of osmosis on the swelling of Eurobitum BW due to water uptake under laboratory conditions and a sensitivity analysis were performed in order to see the effect of the transport parameters (permeability, diffusion and osmotic efficiency coefficients) that control the magnitude of coupled fluxes, principally chemical osmosis and ultrafiltration, on swelling and swelling rate of BW and on $NaNO_3$ leaching.

3 MODELLING OF IN-SITU DISPOSAL SITE

The CHM formulation was used to model the in-situ disposal gallery. The analysis has assumed axis-symmetric conditions. Two different geometries of the modeled domain were considered. Firstly, a section of the disposal gallery in the axial direction has been considered. This two-dimensional axisymmetric case was studied with a rectangular modeled domain. The drums of Eurobitum, the concrete container, the concrete liner, the backfill, and the host rock have been represented. However, this first configuration neglects the existence of joints between the concrete blocks that form the liner. So, secondly in order to avoid such a restriction, a section of the gallery has been taken perpendicularly to the axial direction (Figure 1).

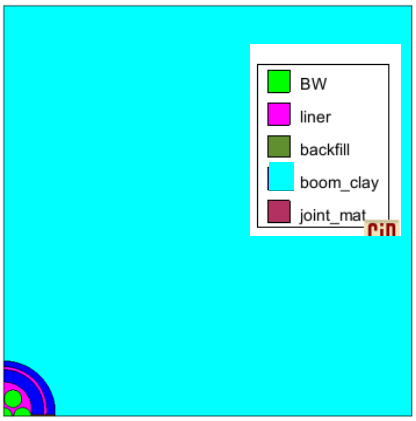

Figure 1 Model Geometry

According to this model, the crystals dissolve and vanish and porosity increases at the outer boundary of the drums after ~2 years while, no change is observed in the middle of the drum after ~10 years (Figure 2). This suggests that it will take several years before the hydration front has reached the center of the drums. The kinetics of water supply will basically be controlled by the permeability of the host clay formation. The degree of saturation and water pressure will increase in the disposal system including the artificial material ensuring a

continuous flow of water towards the BW. Therefore, water pressure increases in the BW. After a few years the pore water pressure in the drums of BW would reach a maximum of ~3 MPa years.

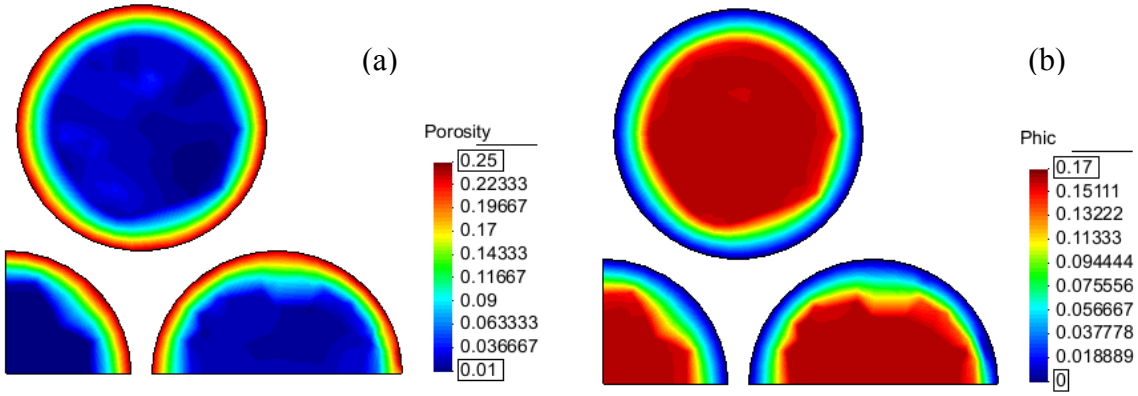

Figure 2 Porosity (a) and crystal distribution (b) in BW drums in disposal gallery after ~10 years

For Eurobitum, in geological disposal conditions, free swelling will only be possible during a first phase, until the free volume in 220 litre drums is filled with swollen material. However, for this simple model configuration this first phase is neglected and pressure increase in the BW drums will induced an increasing stress on the concrete secondary container and on the surrounding Boom Clay. The concentration profile through the Boom Clay after 10 years is shown in Figure 3. Because the BW is not a perfect semi permeable membrane, the solute is allowed to diffuse out of BW and Concentration increases at the outer boundary of the gallery. It is expected that this chemical disturbance will probably have some effects on the mechanical and hydraulic properties of the Boom Clay [2].

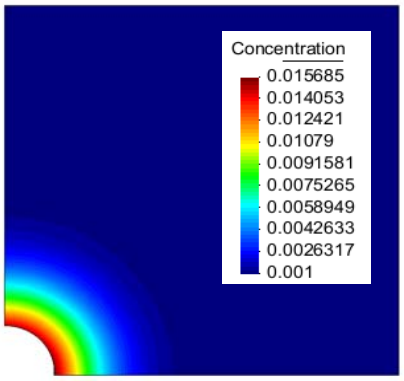

Figure 3 Concentration distribution in Boom Clay after ~10 years

REFERENCES

[1] ONDRAF/NIRAS, 'The Long-term Safety Assessment Methodology for the Geological Disposal of Radioactive Waste', ONDRAF/NIRAS report NIROND TR-2009-14 E (www.nirond.be), (2009).

[2] Mokni, N., (2011) 'Deformation and flow induced by osmotic processes in porous materials' PhD thesis, Universitat politècnica de catalunya, España.

[3] Olivella, S., A. Gens, J. Carrera, E. E. Alonso, 1996, 'Numerical Formulation for a Simulator (CODE_BRIGHT) for the Coupled Analysis of Saline Media " Engineering Computations, Vol 13, No 7, pp: 87-112.

ACKNOWLEDGMENT

This work is funded by NIRAS/ONDRAF, the Belgian Agency for the Management of Radioactive Waste and Fissile Materials.

BUFFER PARAMETER EVALUATION AND MODELLING

Hassan M.M. and Pintado X.

B+TECH Oy, Laulukuja 4, FI-00420, Helsinki, Finland
e-mail: mdmamunul.hassan@btech.fi

Key words: Nuclear waste repository, Buffer, Bentonite MX-80, Oedometer

Abstract. *MX-80 bentonite is considered to be used as a buffer material for the construction of the multiple barrier disposal site for spent nuclear fuel repository. In order to study the Thermo-Hydro-Mechanical (THM) behavior and evaluate material parameter of MX-80 bentonite various laboratory tests have been performed. This study presents very briefly the odeometer test programme and material parameter evaluation. Barcelona Basic Model implemented in CODE BRIGHT has been used for mechanical modeling.*

1 INTRODUCTION

Compacted bentonite is used as a buffer material to make barriers for contamination isolating. High-density compacted bentonite in the form of blocks, discs and rings has also been proposed as sealing material in high-level nuclear waste repositories, as it provides very low permeability, sufficient thermal conductivity and adequate mechanical resistance. To study the functionability of bentonite various hydro-mechanical (HM) tests has been performed. The main purposes of these tests are to study the material behavior and to evaluate material parameters for Thermo-Hydro-Mechanical (THM) modeling of the buffer in the nuclear waste repository.

Barcelona Basic Model (BBM) [1] implemented in finite element code "CODE BRIGHT" [2] has been used to model the hydro-mechanical behaviour of bentonie MX-80 in oedometric condition.

2 EXPERIMENTAL PROGRAMME

2.1 Oedometer Tests

The oedometer test setup is presented in Figure 1a. The cell was made with stainless steel and any radial strain was constrained. During the test axial stress was imposed and uniaxial strain and radial stress were measured. Depending on the test type, the samples were saturated through a porous stone from the bottom of the samples at a constant axial stress. The samples were directly compacted into the cells. Generally, the diameter of the tested samples were 50 mm with minimum height of 20 mm.

Three test paths Path I (A-B-D-B), Path II (A-C-D-B) and Path III (A-C-A), presented in Figure 1b, were considered for the oedometer test programme. Initially the samples were compressed with their initial water content to achieve the desired dry density and this state is presented by A. The most common test path is Path I. After achieving the initial state (A), samples were allowed to hydrate with water at a constant axial stress. After the full saturation samples transform from state A to B, where suction was considered zero. From the B state

conventional loading-un/reloading were performed following the path B-D-B. In the test Path II, samples were tested following the test path A-C-D-B. From the initial state A, samples were loaded to a specified stress level to reach state C. The suction of the sample increases as the samples were loaded. The change in suction was considered negligible as the stress level was not very high in magnitude to change suction properties drastically. From state C samples were then hydrated with water following the path C-D, where suction can be considered as approximately zero. The third test path Path III (A-C) is the first phase of the test Path II.

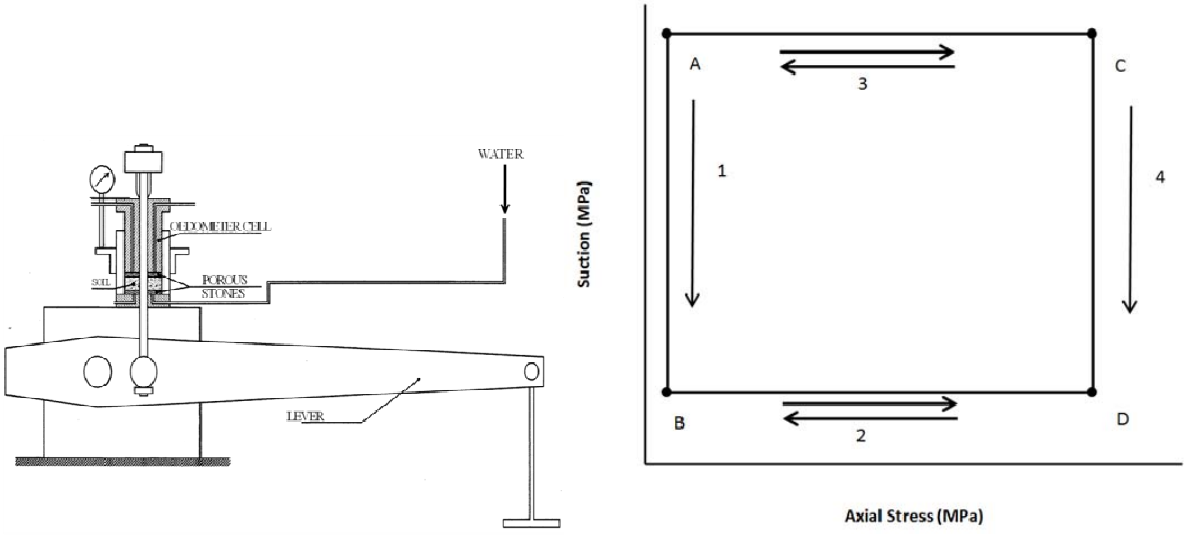

Figure 1. (a) Schematic of Oedometer test set-up and (b) test path of the experimental programme

Three tests have been selected for this study and Table 1 presents the initial condition of the tested material. The material had initial water content around 6 % and initial target density was 1 600 kg/m^3**.** The suction of the tested samples varied from 150 to 220 MPa approximately.

Test ID	Initial conditions			Test Path	Salinity (%)
	Dry density (kg/m^3)	Initial water content (%)	Suction (MPa)		
100212c	1600	6.0	153.3	A-B-D-B	0
101222d	1590	6.0	218.6	A-C-D-B	7.0
100212a	1590	6.0	153.3	A-C	-

Table 1: Initial condition of the bentonite MX-80 samples

2.2 Material model and parameters

The Thermo-elastoplastic (TEP) model of CODE BRIGHT is used in this study. Material parameter and relationship have been evaluated according to [3] and [4]. A strategy to evaluate material parameters is now under development, presented in Figure 2, and material parameter used in this modeling, is presented in Table 2.

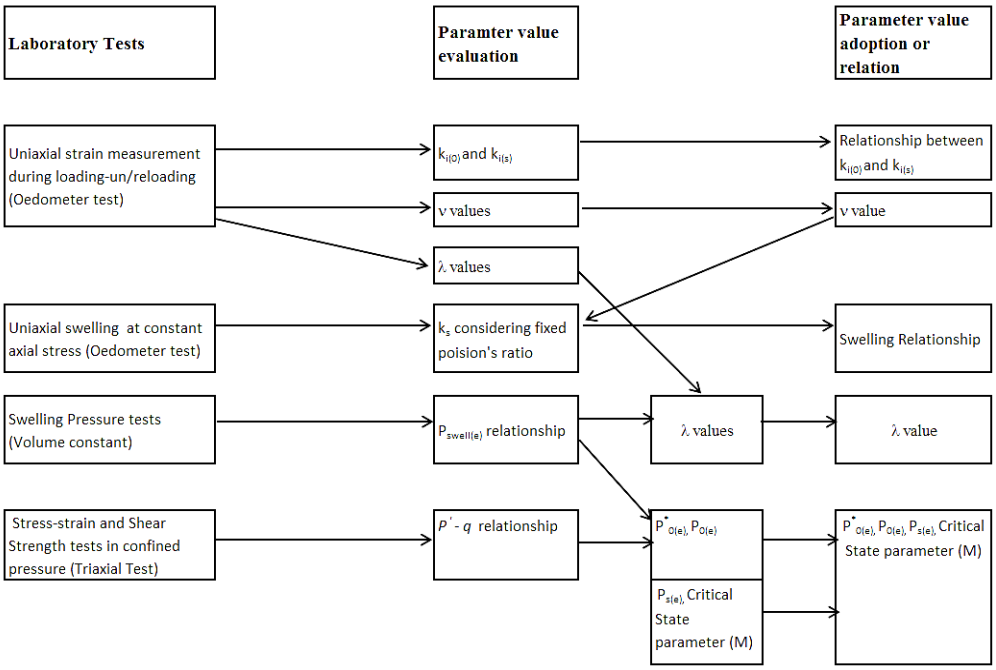

Figure 2. Mechnical Parameter evaluation strategy

Parameter	Test Id	100212c	101222c/ 101222d		100212 101222c	101222d
Elastic	κ_{i0}	0.08		Plastic	λ(0)	0.18
	α_i	0.006			r	0.8
	κ_{s0}	0.25			β	0.04
	α_{sp}	0.525	0.22		p_{s0}	0.5
	ν	0.25			p^c	0.01
	K_{min}	20			M	0.35
	p_{ref}	0.1			α	0.5
					e_0	0.6
					p^*_0	0.65

Table 2. Parameter used for modelling

2.3 Model geometry and boundary conditions

Radial displacements were restricted along the vertical boundaries and no vertical displacement was allowed at the bottom boundary to represent the oedometric condition. A constant axial stress was imposed on the horizontal upper boundary and hydration allowed depending on the test path both on the top and bottom boundaries. 2D axisymmetric mesh was used in the modeling.

3 RESULTS AND DISCUSSION

Figure 3 presents the stress-strain behavior of the oedometer tests and the modeling results. Stress-strain modeling results follows the 100212c test path in relatively good agreement though swelling strain is less than the real test. For the test paths 101222c and 101222d modeling results follows the average stress-strain line before swelling. The swelling strain at the high stress level is also in good agreement with the test 101222d, though it should be noted that saline water (3:2 Ca^{+2}/ Na^{+}) was used in the test.

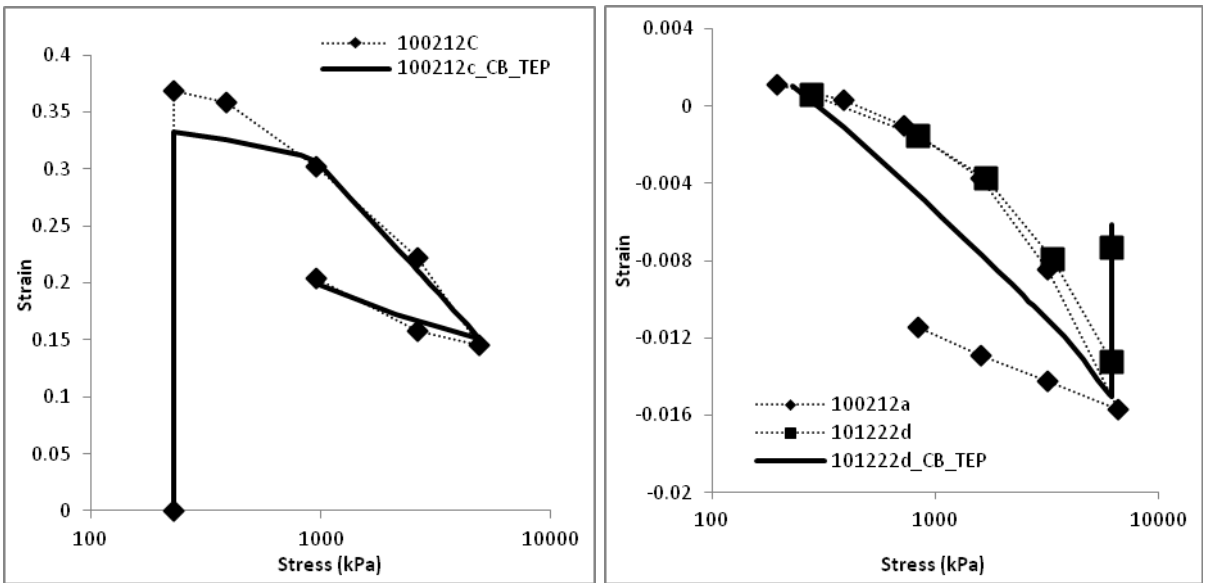

Figure 3. Oedometer test and modeling results

4 CONCLUSIONS

Hydro-mechanical beahviour of the tested material is presented briefly. Parameter evaluation and finite element modeling are also presented. It is in the planning stage to perform triaxial test to study the material behavior.

Despite the limitation of the BBM, the initial modeling test results shows the TEP model can evaluate these simple test path in relatively good agreement.

Acknowledgements

This work is commissioned and supported by Posiva Oy in Finland.

REFERENCES

[1] Alonso E.E., Gens A and Josa A, 1990. A constitutive model for partially saturated soils. Géotechnique, 40(3): 405-430.

[2] Olivella, S., Gens, A., Carrera, J., Alonso, E.E., (1996). Numerical formulation for a simulator (CODE-BRIGHT) for the coupled analysis of saline media. Eng. Comput. 1: 87– 112

[3] Hassan, M.M., Pintado, X., and Martikainen, J. (2012). Thermo-Hydro-Mechanical Laboratory Tests on MX-80. Posiva report (under preparation). Eurajoki.

[4] Åkesson M, Börgesson L, Kristensson O, 2010. SR-Site Data report. THM-modelling of buffer, backfill and other system components. SKB Report in prep, Svensk Kärnbränslehantering AB.

EVALUATION OF GROUNDWATER FLOW IN NUCLEAR WASTE REPOSITORIES

Pintado X. and Autio J.

B+TECH Oy, Laulukuja 4, FI-00420, Helsinki, Finland
e-mail: xavier.pintado@btech.fi

Key words: Nuclear waste repository, hydraulic conductivity, fractures

Abstract. *The nuclear waste repository reference in Finland in Olkiluoto is constructed in crystalline rock. The canisters with the spent fuel are in holes surrounded by bentonite, swelling clay. The groundwater flow from the rock hydrates the clay and the clay swells and seals the repository. The rock is a complex system because there are fractures with different sizes and orientations, so there is a wide range of hydraulic permeabilites and anisotropies in rock and it is necessary looking for equivalent properties in the constitutive laws available in CODE_BRIGHT which take into account the special properties of a crystalline fractured rock.*

1 INTRODUCTION

Compacted bentonite is used as a material to make barriers to prevent contamination isolating the contamination source. High-density compacted bentonite in the form of blocks, discs and rings has also been proposed as sealing material in high-level nuclear waste repositories, as it provides very low permeability, sufficient thermal conductivity and adequate mechanical resistance. This compacted bentonite is surrounded by a crystalline rock. The groundwater flows through this rock and hydrates the clay.

The groundwater flow in Olkiluoto has been modeled with different ways. It has been simulated by other authors under some assumptions of discrete media like DFN model (discrete fracture network) [1] or dual porosity model [2] and continuous model with fractures into the continuous media (EPM, equivalent porous medium model) [2]. These models allow modeling the groundwater flow to the tunnels and deposition holes and evaluating the water flux to the backfill tunnels and deposition holes.

The problem has been simulated with CODE_BRIGHT [3]. This code cannot simulate fractured planes, so the crystalline rock has been considered as a continuous media with discrete fractures, which are simulated as a continuous media with width and hydraulic conductivity equivalent to transmissivity. Trial and error method has been used for checking the value of the rock and three fractures hydraulic conductivities fixing hydrostatic liquid pressure in the model boundaries and atmospheric pressure in the empty tunnels. The calculated flow and the flow calculated with regional groundwater models [5-6] are compared for adjusting the rock hydraulic conductivity.

2 MODEL DESCRIPTION

2.1 Geometry

Four different geometries have been used in these calculations (see figure 1):

- Fractures: 6537 nodes and 18573 tetrahedral elements. This geometry has been used for fracture hydraulic conductivity calculations. The width considered has been 200 mm. The flow to the tunnel taken from DFN calculations.
- Single deposition hole 2D axisymmetry: 3272 nodes and 6288 triangular elements. The liquid pressure was fixed at top and bottom boundaries and impermeable lateral border was assumed because of symmetry.
- Single deposition hole 3D: 4890 nodes and 19743 tetrahedral elements. This calculation has been done for checking the effect of the axisymmetric assumption.
- Backfill tunnel and deposition holes: 67310 nodes and 286613 tetrahedral elements. This calculation has been done for checking the effect of the fractures and the backfill boundaries.

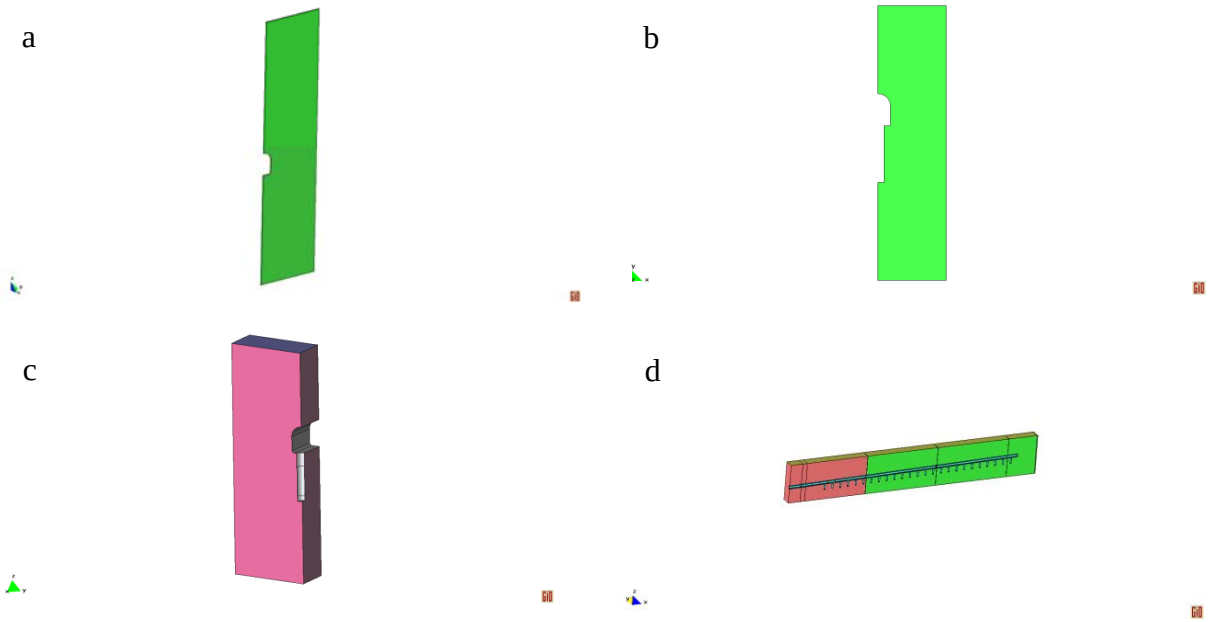

Figure 1. Geometries: a: fracture, b: single deposition hole 2D axisymmetric, c: single deposition hole 3D, d: backfill and deposition holes

2.2 Material parameters

Only the rock and three fractures have been considered in the calculations. The regional groundwater flow models consider the tunnels empty. The most important parameter is the hydraulic conductivity because of although some ventilation effect could dry a small skin around the excavation; it is not expected important effect, so the water retention curve and the relative permeability don't play any role in these calculations because of the rock is always saturated. Ventilation effect in tunnels has been studied in VE test in Monterri [4].

The porosity considered has been 0.02 (total porosity). This parameter doesn't play any role because all calculations considered are in steady state conditions.

The reference hydraulic conductivity for the rock is 1.52×10^{-12} m/s, calculated from [2] and taking into account the presence of fractures with their transmissivity.

2.3 Boundary conditions

The liquid pressure was fixed at top and bottom rock boundaries and impermeable lateral border was assumed because of symmetry. The excavated face boundary condition was atmospheric liquid pressure (0.1 MPa).

3 SIMULATION RESULTS

Three different cases have been analyzed for flow to backfill tunnel through the fractures. The fractures 1-3 have the 10% of total flow and the fracture 2 the 90% (see table 1).

Table 1. Fracture transmissivities

	Fracture 1 (m^2/s)	Fracture 2 (m^2/s)	Fracture 3 (m^2/s)
Wet tunnel (5 l/min)	$6.41x10^{-9}$	$1.17x10^{-7}$	$6.52x10^{-9}$
Typical tunnel (0.5 l/min)	$6.41x10^{-10}$	$1.17x10^{-8}$	$6.52x10^{-10}$
Dry tunnel (0.01 l/min)	$1.28x10^{-11}$	$2.34x10^{-10}$	$1.3x10^{-11}$

The trial and error calculations presented in table 2 have been done for axisymmetric geometry and different flows to deposition holes calculated with a regional groundwater flow model [5-6].

Table 2. Hydraulic conductivity with different flows. Axisymmetric geometry

Case	k (m/s)	Flow (l/min)	Height
1	$3.53x10^{-10}$	0.1	38
2	$3.53x10^{-12}$	0.001	38
3	$3.53x10^{-13}$	0.0001	38
4	$3.53x10^{-15}$	0.000001	38
5	$1.52x10^{-12}$	0.000431	38
6	$1.52x10^{-12}$	0.000604	25
7	$1.52x10^{-12}$	0.000185	100

The flow calculated in case 5 have been compared with the flow in single deposition hole 3D the inflow is 0.00033 l/min (77% of the axisymmetric geometry). In case of backfill tunnel and deposition holes, the liquid flow in deposition holes varies from 0.00035 to 0.00024 l/min (56-81% approximately), see figure 2.

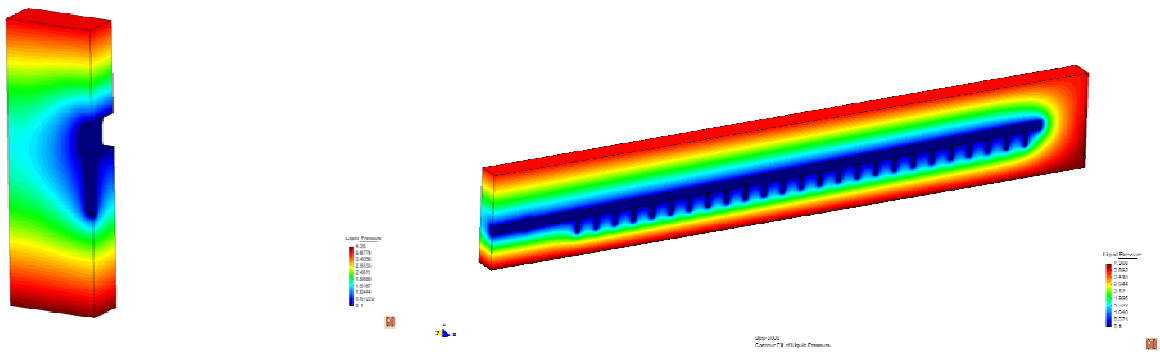

Figure 2. Liquid pressure in steady state conditions. 3D geometries

4 CONCLUSIONS

- The groundwater flow in fractures around nuclear waste repositories can be simulated although there are limitations because of the size of the elements, so only the important fractures can be taken into account.
- The groundwater flow in backfill tunnel and deposition holes results from regional groundwater flow are used for fixing the hydraulic conductivity in near field around the repository. These results come from a discrete fracture network and the equivalent rock hydraulic conductivity is calculated with trial and error method.
- The surfaces where the liquid pressure is fixed must be clearly defined in order to have good hydraulic conductivity values. The hydraulic conductivity decreases when the boundaries are nearer the repository (higher gradients for the same flow).
- The rock hydraulic conductivity can be used for ulterior simulations where the presence of the canister, buffer and backfill is taken into account.
- The 2D axisymmetric geometry underestimates the effect of the backfill tunnel in drainage.

Acknowledgements

This work is commissioned and supported by Posiva Oy in Finland.

REFERENCES

[1] Hartley, L., Jaap Hoek, J., Swan, D.,Roberts, D. (2010). Hydrogeological Discrete Fracture Network Modelling of Groundwater Flow Under Open Repository Conditions. Posiva Working report 2010-51. Eurajoki.

[2] Löfman, J., Poteri, A., Pitkänen, P. (2010). Modelling of Salt Water Upconing in Olkiluoto. Posiva Working report 2010-25. Eurajoki.

[3] Olivella, S., J. Carrera, A. Gens, E. E. Alonso, 1994a. Non-isothermal Multiphase Flow of Brine and Gas through Saline media. Transport in Porous Media, 15, 271:293

[4] Mayor, J.C., Velasco, M., García-Siñeriz, J.L. (2006). Ventilation experiment in the Mont Terri underground laboratory. Physics and Chemistry of the Earth, 32:616-628

[5] Hellä, P. (2011). Inflow to deposition holes and repository tunnels. Memorandum Project-1042-X/2011. Saanio&Riekkola. Helsinki.

[6] Hellä, P. (2011). Revision of the target properties for host rock. Memorandum Project-1042-2/2011. Saanio&Riekkola. Helsinki.

PHYSICAL MODELLING AND NUMERICAL SIMULATION OF COMPACTED SALT BACKFILL USING CODE_BRIGHT

O. Czaikowski, K. Wieczorek, C.-L. Zhang, and K.-P. Kröhn

Gesellschaft für Anlagen und Reaktorsicherheit (GRS) mbH
Theodor-Heuss-Strasse 4, 38122 Braunschweig, Germany
e-mail: oliver.czaikowski@grs.de, web page: http://www.grs.de

Key words: crushed salt, long-term compaction behaviour, FADT

Abstract. *Crushed salt is the intended buffer/backfill material around the casks and canisters in a geologic repository for HLW in rock salt. An enhanced understanding of the compaction process is required because of the change in the philosophy of safety assessment to the concept of the "Containment Providing Rock Zone". In this paper numerical modelling work, reflecting the load and time dependent properties of the salt backfill is shown. Results of new laboratory experiments performed at the GRS laboratory are currently used to investigate different deformation mechanisms and to derive and qualify material parameters needed for the numerical simulation. The results of this work, as far as they are available to date, are presented in this paper.*

1 INTRODUCTION

In the last decade the safety concept in Germany for the geologic disposal of HLW in rock salt has been refined. The change in the philosophy of safety assessment to the concept of the "Containment Providing Rock Zone" influenced the importance of different components in a salt repository. In particular, the role of crushed salt as the intended buffer/backfill material around the emplaced casks and canisters became more prominent. An increase of understanding of the compaction process is required for this material. Therefore, the project REPOPERM was initiated to address the question about the hydraulic and mechanical behaviour of the salt backfill at low porosities.

In phase 1 the available data were reviewed in this respect. The results demonstrated a significant data scattering, partly due to lithological effects, but also as a consequence of different fluids used to hydraulic testing. In the framework of the preliminary safety case for the Gorleben salt dome a suggestion has been made that at lower porosities (i.e. < 10%) only permeabilities measured with salt solution seem to be relevant.

Available material parameters were used for preliminary modelling of the THM-coupled long-term evolution of the crushed salt backfill for borehole disposal. It was, however, found that a further qualification of constitutive laws and material parameters is needed for reliable modelling.

In phase 2 a laboratory program was designed to achieve this for the advanced but still measurable range of compaction as far as possible. The validity of material parameters at even lower porosities which elude direct measurement is discussed in Kröhn et al. (2012).

In this paper numerical modelling work, reflecting the load and time dependent properties of the salt backfill is shown. Results of new laboratory experiments performed at the GRS laboratory are currently used to investigate different deformation mechanisms and to derive and qualify material parameters needed for the numerical simulation.

The results of this work, as far as they are available to date, have already been presented at SaltMech7 conference in Paris in April 2012 (Czaikowski et al. (2012)).

2 PHYSICAL MODELING AND NUMERICAL SIMULATION

The computer code CODE_BRIGHT developed by the Technical University of Barcelona (UPC) is used by GRS for analysis of coupled thermo-hydro-mechanical (THM) phenomena in geological media. The development of CODE_BRIGHT started in the 1990's with the purpose of modelling the response of saline materials in the context of underground nuclear waste disposal. The initial capabilities were soon extended to a wider range of geological and technical materials and, in particular, unsaturated soils CODE_BRIGHT (2002).

A constitutive model for crushed salt was implemented that contains both time-independent deformation as well as viscous material behaviour Olivella & Gens (2002). A viscoplastic term was intended for modelling non-creep deformation mechanisms such as grain re-organization and crushing. In addition, a creep constitutive model was developed that is based on two different viscous deformation mechanisms: dislocation creep and fluid-assisted diffusional transfer. The latter was able to describe the acceleration of the compaction process of crushed salt samples in laboratory tests when a small amount of brine is added.

2.1 Physical modelling of crushed salt

The total deformation rate of the crushed salt is calculated as the sum of contributions from the different deformation mechanisms:

$$\dot{\varepsilon}_{CS} = \dot{\varepsilon}^{EL} + \dot{\varepsilon}^{DC} + \dot{\varepsilon}^{VP} + \dot{\varepsilon}^{FADT} \tag{1}$$

The different contributions are presented in the following sections.

2.1.1 Elastic deformation behaviour

Crushed salt is considered isotropic with regard to elastic deformation, i.e. following Hooke's law elastic deformation can be described by two independent variables. CODE_BRIGHT uses Young's modulus E and Poisson's ratio ν.

While Poisson's ratio is considered as independent from the degree of compaction, E can be given as a linear function of porosity η:

$$E = E_0 + (\eta - \eta_0)\frac{dE}{d\eta} \tag{2}$$

with constants E_0 and η_0.

2.1.2 Dislocation creep

Dislocation creep is a time-dependent deformation mechanism describing the strain inside the salt crystals under deviatoric stress conditions. It has been widely studied for competent rock salt (e.g., Wallner et al. (1979), Hunsche (1984)). In the original form, volumetric deformation is not possible. Olivella & Gens (2002) proposed a modification that enables volumetric deformation, i.e., creep compaction, for materials with significant porosity. Under steady-state conditions the mathematical description takes the form CODE_BRIGHT (2002)

$$\dot{\varepsilon}_{ij}^{DC} = \frac{1}{\mu_{dev}^{DC}} \cdot \Phi(F) \cdot \frac{\partial G}{\partial \sigma'} \tag{3}$$

where $\Phi(F) = F^n$ with stress exponent n and the stress function F and flow rule G

$$G = F = \sqrt{q^2 + \left(\frac{-p'}{\alpha_p}\right)^2} \tag{4}$$

where q and p' are the deviatoric stress and the mean effective stress, respectively, and the material parameter α_p is given by

$$\alpha_p = \left(\frac{\mu_{vol}^{DC}}{\mu_{dev}^{DC}}\right)^{1/(n+1)} \tag{5}$$

with the void ratio (e) dependent viscosities

$$\frac{1}{\mu_{vol}^{DC}} = A(T) \cdot g_{vol}^{DC}(e) \tag{6}$$

$$\frac{1}{\mu_{dev}^{DC}} = A(T) \cdot g_{dev}^{DC}(e) \tag{7}$$

Temperature dependence is given by

$$A(T) = A_A \cdot \exp\left(\frac{-Q_A}{R \cdot T}\right) \tag{8}$$

with structural parameter A_A, activation energy Q_A, universal gas constant R, and absolute temperature T.

The void ratio functions are defined by

$$g_{vol}^{DC}(e) = 3 \cdot (G-1)^n \cdot f \tag{9}$$

$$g_{dev}^{DC}(e) = \left(\sqrt{\frac{1+g+g^2}{3}}\right)^{n-1} \cdot \left(\frac{2 \cdot g + 1}{3}\right) \cdot f + \frac{1}{\sqrt{g}} \tag{10}$$

where

$$g = \frac{1}{(1-f)^2} \text{ and } f = \sqrt{\frac{2e}{3 \cdot (1-e^{3/2}) \cdot (1+e)}} \tag{11}$$

2.1.3 Viscoplastic TM-coupled deformation behaviour (grain re-organization and crushing

While dislocation creep describes the inelastic deformation of the individual salt grains, the viscoplastic behaviour of the grain aggregate is represented by the following formulation CODE_BRIGHT (2002).

$$\dot{\varepsilon}_{ij}^{VP} = \Gamma \cdot < \Phi(F) > \frac{\partial G}{\partial \sigma} \tag{12}$$

where $\Phi(F) = F^m$ for $F > 0$ and $\Phi(F)=0$ otherwise.

The yield function and flow rule are defined as

$$G = F = q^2 - \delta^2 (p_0 \cdot p' - p'^2) \tag{13}$$

with the mean effective stress p' and the deviatoric stress q and the parameter δ. The temperature-dependent viscosity Γ is given by

$$\Gamma = \Gamma_0 \cdot \exp(\frac{-Q}{R \cdot T}) \tag{14}$$

Hardening is expressed by the variation of the pressure p_0 with the volumetric deformation ε_V:

$$dp_0 = D \cdot l \cdot \varepsilon_V^{l-1} \cdot d\varepsilon_V \tag{15}$$

with the parameters D and l.

2.1.4 THMC-coupled viscous deformation behaviour (FADT)

From experimental observations it is known that crushed salt containing an amount of brine behaves considerably softer than dry crushed salt. The mechanism which is held responsible for this is pressure solution at the contact zones between the grains, where stress concentrations occur, and precipitation in the pores. It was described by Spiers et al. (1986, 1990) and implemented in CODE_BRIGHT Olivella & Gens (2002). In contrast to the other time-dependent deformation mechanisms, the deformation rate is linearly dependent on stress:

$$\dot{\varepsilon}_{ij}^{FADT} = \frac{1}{2\mu_{dev}^{FADT}} (\sigma'_{ij} - p' \cdot \delta_{ij}) + \frac{1}{3\mu_{vol}^{FADT}} p' \cdot \delta_{ij} \tag{16}$$

with the deviatoric and volumetric viscosities μ_{dev} and μ_{vol} and Kronecker's symbol δ_{ij}. The viscosities are functions of temperature, saturation, porosity or void ratio, and grain size.

$$\frac{1}{\mu_{vol}^{FADT}} = \frac{16B(T)\sqrt{S_l}}{d_0^3} g_{vol}^{FADT}(e) \tag{17}$$

$$\frac{1}{2\mu_{dev}^{FADT}} = \frac{16B(T)\sqrt{S_l}}{d_0^3} g_{dev}^{FADT}(e) \tag{18}$$

with liquid saturation S_l and d_0 as a grain size parameter.

Temperature dependence is given by the function $B(T)$:

$$B(T) = \frac{A_B}{R \cdot T} \cdot \exp(\frac{Q_B}{R \cdot T}) \tag{19}$$

with the parameters A_B and Q_B.

Finally, the dependence on the void ratio e is obtained by

$$g_{vol}^{FADT}(e) = \frac{3g^2 \cdot e^{3/2}}{1+e} \text{ and } g_{dev}^{FADT}(e) = \frac{g^2}{1+e} \tag{20}$$

where g is the same as in equation (11).

2.2 GRS laboratory investigations on long-term deformation behaviour of crushed salt

A number of parameters associated with the above equations are material specific parameters which are to be determined by laboratory experiments. Based on Kröhn et al.

(2009) the material parameters associated with the constitutive equations implemented in CODE_BRIGHT were determined for crushed salt and used in the first step of the documented calculations. In order to qualify these parameters, additional laboratory experiments were planned and are currently being performed. For numerical analysis of the behaviour of the crushed salt during these laboratory tests according to Kröhn et al. (2012) an axisymmetric configuration centred in the axis of the sample has been considered. The sample is h0 = 110 mm in height and d0 = 120 mm in diameter. In addition, the steel piston is explicitly modelled with a height of h0 = 340 mm and a diameter equal to the sample diameter.

The time-depending compaction behaviour of crushed salt is investigated by GRS in the framework of the project REPOPERM phase 2. The samples have been compacted by hand down to porosity values of about 30 % before starting the test.

The testing sequence starts with a very low axial stress of 1 MPa over 50 days, before increasing the axial stress in steps of 3 MPa.

The stress boundary conditions applied to the two different samples are shown in figure 1. Due to the applied stress conditions the samples show time-dependent deformation behaviour. The decrease of the sample height is observed and used for re-calculation of the porosity change. The change of the porosity with time is shown in figure 2.

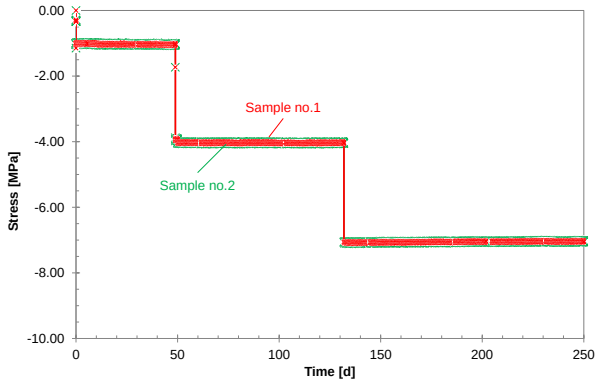

Figure 1: Stress boundary conditions during testing

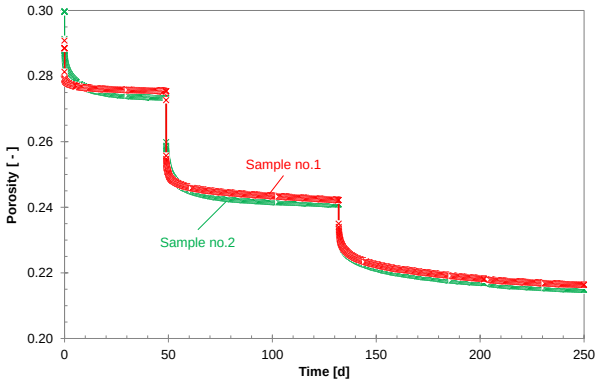

Figure 2: Development of porosity during testing

2.3 Back calculation of lab test results – data set related to the BAMBUS project

In a first step, the parameter set determined in the framework of the BAMBUS projects Bechthold et al. (2004) and calibrated by simulating lab test results from BGR, e.g. Stürenberg (2004) was used for the back calculation of the experiment. The testing procedure was calculated with CODE_BRIGHT. The results from numerical simulation are compared to the measured values.

In figure 3 the experimental data and the corresponding simulation results for sample no.1 are shown. Porosity change is plotted as a function of time. Figure 4 shows the corresponding plot for sample no.2.

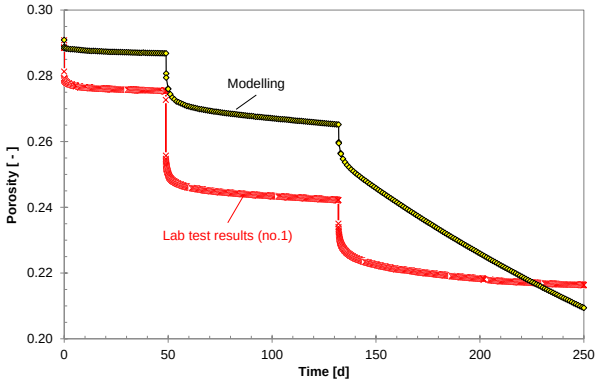

Figure 3: Back calculation of lab test results of sample no.1

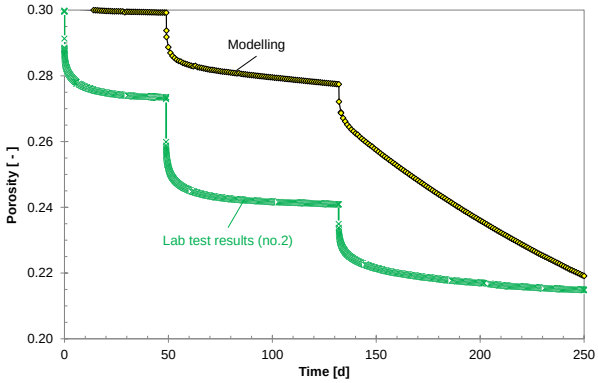

Figure 4: Back calculation of lab test results of sample no.2

Regarding these figures it is obvious that both, the transient as well as the stationary deformation behaviour of the samples could not be reproduced by numerical modelling with this parameter set. The results from numerical simulation underestimate the transient deformation behaviour whereas the stationary deformation behaviour is highly overestimated.

It has to be noted that the BGR tests were not originally planned for serving as model calibration experiments. Aiming on the strength of the granular salt with respect to its backfill behaviour a large number of oedometer tests at controlled strain-rate conditions were performed. A specific experimental testing procedure was used to estimate the strength-porosity relationship. This test type represented a mixture of various overlapping processes, e.g., elasto-plastic and time-depending processes.

Therefore, separation of the various processes with respect to calibration of the employed models proved problematic.

In the second step which is currently on-going, the data set has to be reviewed with respect to long-term deformation behaviour. The results of this validation process, as far as they are available to date, are shown in the following paragraph.

2.4 Back calculation of lab test results – validation process

When comparing measured experimental data to results from numerical modelling within a reliable validation process the first step is to care for identical boundary conditions. From the testing results in figure 1 it is obvious that with increasing axial load after the first testing phase with low axial stress, the two samples show similar deformation behaviour during the following load steps. To eliminate the influence of the sample preparation the first 50 days are not taken into account for the validation process. In fact this period could be seen as a pre-testing consolidation phase, similar to a re-compaction phase used in classical laboratory tests on competent samples.

In figure 5 the adapted experimental data for sample no.1 and sample no.2 are shown in terms of porosity decrease with time. The figure is almost identical to figure 2, except for the shifted time axis and the latest data added.

The simulation results of sample no.1 as well as the experimental data achieved so far are shown in figure 6.

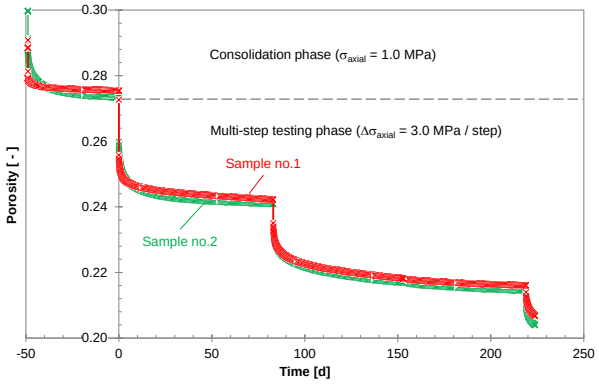

Figure 5: Development of porosity during testing

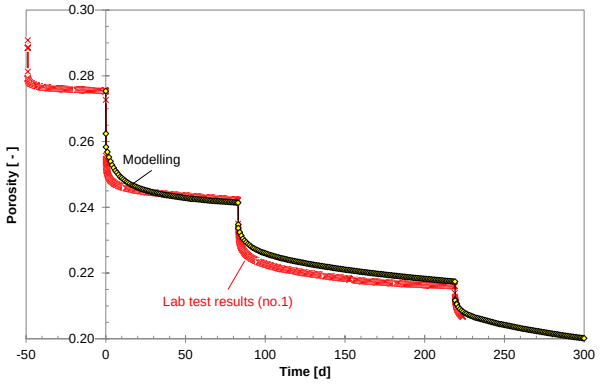

Figure 6: Back calculation of lab test results of sample no.1 using the validated parameter set

The next step within the validation process is the separation of the various processes with respect to the used constitutive laws and their depending material parameters as far as possible. Therefore, in table 1 only the final parameter set is given that is currently used to numerically simulate the laboratory tests. This set seems to be adequate for describing the experimental results obtained so far.

Table 1. Material parameters determined for crushed salt

Elastic deformation behaviour		
E_0	1.00	MPa
η_0	0.30	-
E_0/η_0	-4.50E+03	MPa
ν	0.27	-
Dislocation creep		
A_A	2.08E-06	$s^{-1}MPa^{-n}$
Q_A	5.40E+04	J mol^{-1}
n	5.00	-
Viscoplastic deformation behaviour		
δ	10.00	-
Γ_0	7.00E-04	s^{-1}
Q	5.40E+04	J mol^{-1}
p_0	0.10	MPa
D	1.00E+05	MPa
l	4.00	-

2.5 Back calculation of lab test results – separation of overlapping processes

For numerical analysis and reliable interpretation of the time-dependent behaviour of drifts in rock salt when backfilled with crushed salt it is of great importance to be able to separate the overlapping processes in time and space. Therefore the deformation processes that lead to the plotted porosity development shown in figure 7 can be separated with respect to the used constitutive laws.

In figure 7, figure 6 is extended by the different simulation results for (1) elasticity only, (2) elasticity and dislocation creep, (3) elasticity and viscoplasticity.

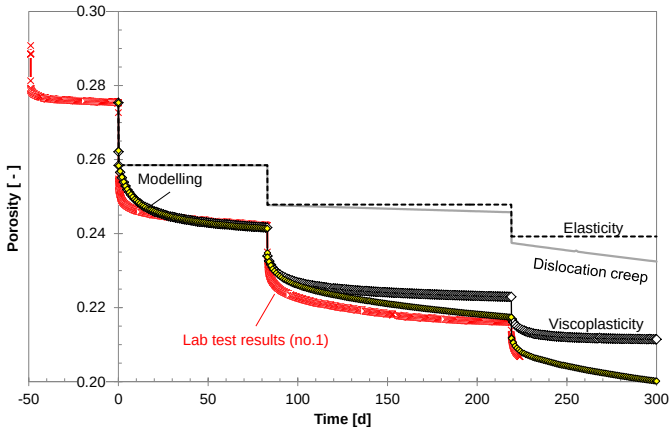

Figure 7: Back calculation of lab test results of sample no.1 with respect to the used different constitutive laws

From the testing results shown in figure 7 it is obvious that the porosity change observed within the first loading step of 4 MPa could be simulated only by using the viscoplastic constitutive approach together with the elastic law. Whereas for simulating the porosity development within the following loading steps the consideration of the dislocation creep approach is imperative.

2.6 Influence of moisture on long-term deformation of crushed salt

It is known from experimental observations according to Kröhn et al. (2009, 2012) that crushed salt containing an amount of brine behaves considerably softer than dry crushed salt. This effect could be distinctly represented in the results from preliminary THM-coupled numerical simulations Czaikowski et al. (2012).

In the framework of the project REPOPERM phase 2 GRS is investigating the long-term deformation behaviour of wetted crushed salt samples in parallel to the presented dry ones. Within the validation process of the used constitutive laws presented in this paragraph and their related material properties, the laboratory tests are back-calculated by numerical modelling and the simulation results are compared to the experimental findings. However, the results achieved so far look promising but still have to be discussed internally.

3 CONCLUSIONS

Crushed salt is the intended buffer/backfill material in a geologic repository for HLW in rock salt. A profound understanding of the thermal-hydraulic-mechanical behaviour of this material is needed for reliable prediction of the repository evolution. This is the subject of the on-going project REPOPERM. The available data for crushed salt are presented and analysed in Kröhn et al. (2012).

The work presented here aims at the evaluation of numerical modelling capabilities for the long-term deformation backfill behaviour, especially with regard to the computer code CODE_BRIGHT employed by GRS. Several constitutive models are available, and different aspects of material behaviour can be modelled separately. The discrimination between the contributions of different mechanisms is particularly useful. It allows the calibration of the material parameters for each mechanism by performing and simulating respective tests.

This calibration is currently in process. The results shown here have been obtained with the

first calibration cycles. A problem with calibration is the sparseness of relevant test data. This problem is also addressed in Kröhn et al. (2012). Obviously, calibration can only be as good as the input data.

Some confirmation in the case of dry compacting material and, in particular, additional experimental evidence in the case of moisture-containing backfill is clearly needed. Laboratory experiments and a modelling exercise making use of these experiments as well as supplemental microstructural investigations are presently underway to build up confidence in a fully coupled THM-model for compacting crushed salt.

4 ACKNOWLEDGEMENTS

The authors gratefully acknowledge the funding by the German Ministry of Economics and Technology (BMWi) under contract no. 02 E 10477 and 02 E 10470.

REFERENCES

Bechthold, W., E. Smailos, S. Heusermann, W. Bollingerfehr, B. Bazargan Sabet, T. Rothfuchs, P. Kamlot, J. Grupa, S. Olivella, and F.D. Hansen (2004): Backfilling and Sealing of Underground Repositories for Radioactive Waste in Salt (BAMBUS-II Project). EUR 20621, European Commission, Brussels.

CODE_BRIGHT (2002): A 3D program for thermo-hydro-mechanical analysis in geological media. Users guide

Czaikowski, O., Wieczorek, K., Kröhn K.-P. (2012). Compaction of salt backfill – new experiments and numerical modelling. 7th Conference on the Mechanical Behavior of Salt. 16th -19th April 2012, MINES ParisTech, Paris.

Hunsche, U. (1984): Results and Interpretation of Creep Experiments on Rock Salt. Proc. of the 1st Conf. Univ. Park (USA) 1981. Eds.: Hardy, H.R. Jr & Langer, M.: 159-167, Trans Tech Publications, Clausthal.

Kröhn, K.-P., Stührenberg, D., Herklotz, M., Heemann, U., Lerch, C., Xie, M. 2009. Restporosität und -permeabilität von kompaktierendem Salzgrus-Versatz; Projekt REPOPERM - Phase 1. Report GRS-254. Braunschweig: GRS.

Kröhn K.-P., Stürenberg, D., Jobmann, M., Zhang, C.-L., Wolf, J. (2012). The compaction behaviour of salt backfill at low porosities. 7th Conference on the Mechanical Behavior of Salt. 16th -19th April 2012, MINES ParisTech, Paris.

Olivella, S. & Gens, A. (2002): A constitutive model for crushed salt. Int. J. Numer. Anal. Meth. Geomech. 26:719-746, 2002

Spiers, C.J., Urai, J.L., Lister, G.S., Boland, J.N., Zwart, H.J. (1986): The influence of fluid-rock interaction on the rheology of salt rock, European Commission, EUR 10399 EN.

Spiers, C.J., Schutjens, P.M.T.M., Brzesowsky, R.H., Peach, C.J., Liezenberg, J.L., Zwart, H.J. (1990): Experimental determination of constitutive parameters governing creep of rock salt by pressure solution, Geological Society Special Publication No. 54: Deformation mechanisms, Rheology and Tectonics, 1990; 215:227.

Wallner, M., Caninenberg, C., Gonther, H. (1979): Ermittlung zeit- und temperaturabhängiger mechanischer Kennwerte von Salzgesteinen. Proc. 4th Int. Congr. on Rock Mechanics, Montreux 1979, Balkema, Rotterdam.

Stürenberg, D. (2004): Compaction and Permeability Behaviour of Crushed Salt and Mixtures of Crushed Salt and Bentonite. Conference Proceedings of DisTec2004, International Conference on Radioactive Waste Disposal, p.511-515, Berlin, April 2004

MODELLING LASGIT EXPERIMENT

S. Olivella*, E.E. Alonso*, D. Arnedo* and C. Hoffmann*

* Department of Geotechnical Engineering and Geosciences
Technical University of Catalonia (UPC-BarcelonaTech)
Campus Norte UPC, 08034 Barcelona, Spain
e-mail: sebastia.olivella@.upc.edu

1 INTRODUCTION

A large scale gas injection test (Lasgit) is carried out at the Äspö Hard Rock Laboratory in Sweden. Lasgit is the first demonstration project designed to study gas migration in bentonite under full-scale repository conditions. The objective of this experimental programme is to provide data to improve process understanding and test/validate modelling approaches, which might be used in performance assessment. Specific objectives are: (1) perform and interpret a large-scale gas injection test based on the KBS-3 repository design concept, (2) examine issues relating to up-scaling and its effect on gas movement and buffer performance, (3) provide additional information on the process of gas migration, and (4) provide high-quality test data to test/validate modelling approaches.

2 TEST DESCRIPTION

Figure 1 shows a schematic representation of the test which among other elements contains a bentonite buffer material constructed using manufactured block rings. The test has a number of injection possibilities, some of them essentially intended for hydration (mat filters above and below canister) and other intended for gas injection (canister wall point sources).

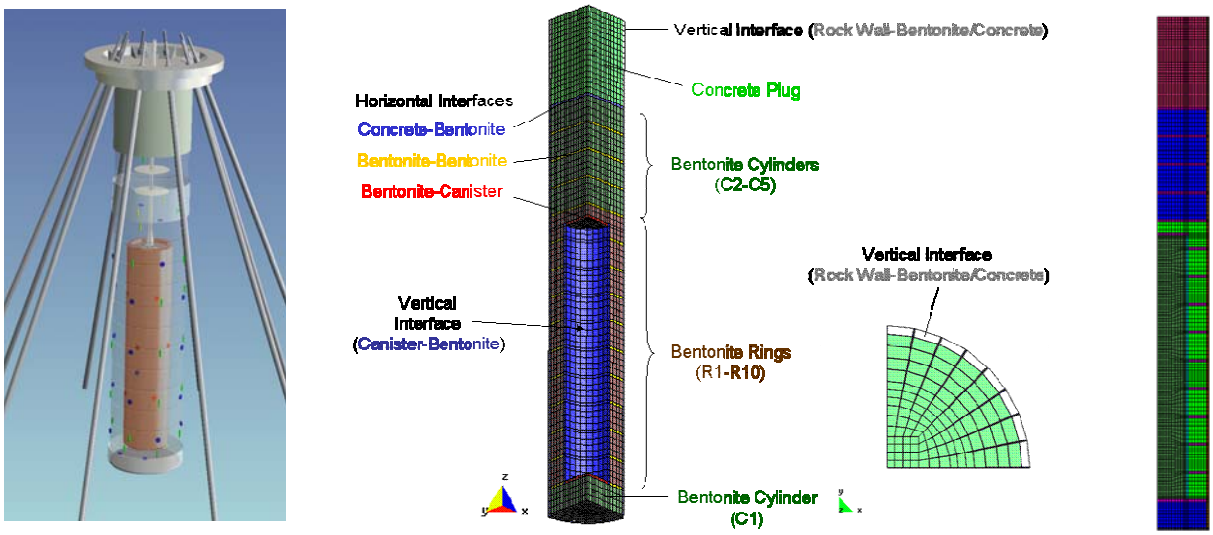

Figure 1. Schematic representation, 3D model and 2D model domains

3 MODELLING AND RESULTS

The modelling work is significantly complex as the water injection phases are extremely fast and thus produce high velocities of water through the interfaces. In a real repository, the interfaces are expected to close when the bentonite expands. However, in a fast test if water penetrates before the saturation of the rings, the opposite effect may be produced, i.e. interfaces opening by pore pressure development.

The modelling of this type of in situ experiments requires the incorporation of a constitutive model that is able to reproduce swelling induced by hydration of the buffer. The installation of the bentonite rings is done in such a way that the contact between the clay blocks and the canister remains as a discontinuity or interface. A similar situation happens on the contact surface between bentonite blocks. It has been observed that under natural hydration (i.e. experiments that do not use forced hydration), these interfaces tend to close as hydration and swelling of the bentonite progresses. Normally, the interface sealing would happen and therefore special treatment of interfaces would perhaps not be necessary. Later, when gas generation by corrosion was generated, these interfaces would play a role and hence they cannot be neglected in a model. The special case of an experiment forces to include the interfaces. The necessity of including the interfaces explicitly appears both for the short term during water injection and for the long term as gas is generated. Even with forced hydration the interfaces manage to close, especially if the bentonite has a high swelling capacity. In case of mixtures of bentonite and sand, the interface closure during an experiment may be compromised as swelling capacity is lower. In any case, gas injection and migration is likely to be controlled by the presence of these interfaces. Therefore modelling of this kind of tests, especially if the water hydration is made very fast, requires the incorporation of interfaces and will improve the capabilities of the model.

The present approach considers interfaces as a zone of a given thickness which contains a so called “embedded” discontinuity model. This is necessary to model the penetration of water during the phase of hydration and later, the pressure responses induced by gas generation. The pressure response at sensors indicates that preferential paths through the discontinuities develop.

As can be seen in Figure 2, gas injection at a point in the canister wall generates a gas propagation front. The gas fluxes are higher at the interfaces than in the bentonite body. The interfaces play a major role as the penetration of the gas takes place in a preferential way. It can be seen that gas pressure development at points situated at some distance increases very suddenly, and at some distance it remains constant. Gas outflow is permitted on the model boundary in a zone representing the fractures of the host rock (the rock is not modelled except for the appropriate boundary conditions representing inflow and outflow).

According to the model, permeability may increase up to two orders of magnitude when the peak of water or gas pressure occurs. Hydration and the induced bentonite swelling counteract the opening effect and therefore, permeability decreases as the interfaces close, going back to low permeability values.

One of the main drawbacks of the axisymmetric model is that the in situ gas injection is performed in reality as point source but in the 2D axisymmetry the point source becomes a

ring source. This reduces the gas pressure increments for the same properties. This also happens for the flows. So developing a 3D model is a necessary but challenging task in view of the complex protocols that are considered in the test.

This work is funded by the EC through the FP7 research program (FORGE Project).

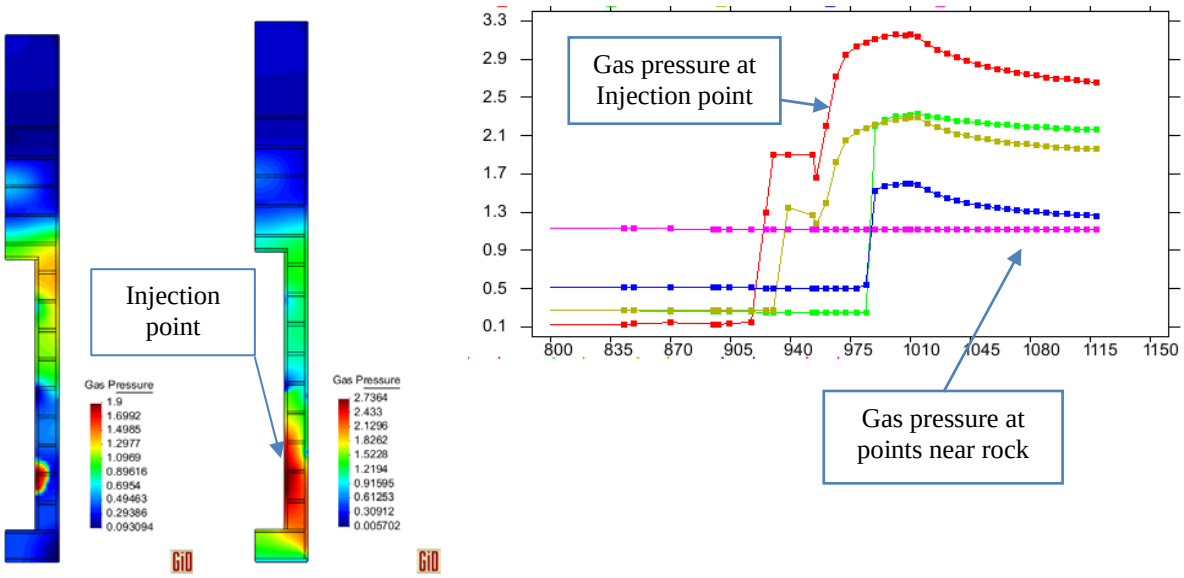

Figure 2. Gas pressure distribution during gas injection and gas pressure evolution at various points

ANALYSIS OF CONVERGENCE OF A THM COUPLED PROBLEM

Nubia A. González[*], Sebastià Olivella[*] and Jean Vaunat[*]

[*] Department of Geotechnical Engineering and Geosciences
Technical University of Catalonia (UPC-BarcelonaTech)
Campus Norte UPC, 08034 Barcelona, Spain
e-mail: code.bright@.upc.edu, web page: http://www.etcg.upc.edu/research/code_bright/

Key words: THM coupled analysis, convergence, time step control

Abstract. *This document contains a study of convergence for a coupled THM problem using CODE_BRIGHT V4. The selected case for the convergence study was the "mock-up" test which involves various non-linear constitutive equations. A tool has been developed to facilitate the convergence analysis of CODE_BRIGHT simulations. The analysis performed shows that the global convergence of the THM problem was very satisfactory. The influence of the option of time step control was also analysed, it was found that the use of a local truncation error tolerance of 10^{-3}-10^{-4}, that is, 0.1-0.01%, is sufficient for most practical applications.*

1 INTRODUCTION

Accurate, reliable and efficient simulations of coupled Thermo-Hydro-Mechanical (THM) problems through porous media are desirable in civil and geo-environmental engineering analysis. This paper focuses on a convergence study of a THM problem using CODE_BRIGHT V4.

Information about the numerical performance of the simulations in CODE_BRIGHT is given in a text file "*root_gen.out*" where residuals of balance equations and variables are given for all time steps, as well as, the current time-step size. For complex problems involving a large number of degrees of freedom or active process modelled (THM), it can be a rather time consuming task to get an overview of the state of the simulation when reading "root_gen.out". To facilitate a more rapid establishment of the convergence state of the simulation, a Matlab program has been developed, which read the information of the file "*root_gen.out*" and organizes data in such way that they can be easily visualized in, for example, Microsoft Excel.

The selected case for the convergence analysis is the "Mockup test" which is a tutorial of CODE_BRIGHT. This is a THM complex case because involves various non-linear constitutive equations. Below a general description of the case and results of the convergence analyses using different options for time step control are given.

2 DESCRIPTION OF THM PROBLEM

The mock-up test addresses the THM response of a highly compacted Bentonite barrier under the combined effects of an artificial outer hydration and an inner heating input. The model geometry is shown in Figure 1, a 2D axi-symmetric longitudinal section is considered. The mechanical behaviour of the clay barrier is simulated using the Thermo-elasto-plastic (TEP) model. The testing procedure involved an initial hydration phase followed by a heating phase in which the following boundary conditions (at the heater boundaries) are imposed:

- from day 0 to day 6, constant power of 250W/heater

- from day 6 to day 20, constant power of 500 W/heater to reach a temperature of 100ºC
- from day 20 to 2500 days, constant temperature of 100ºC

Normally, convergence studies are conducted using dense spatial grids to minimize the influence of errors associated with the numerical approximation of the spatial operator. In this case, the mesh selected is structured and it is made of 304 linear quadrilateral elements (Figure 1).

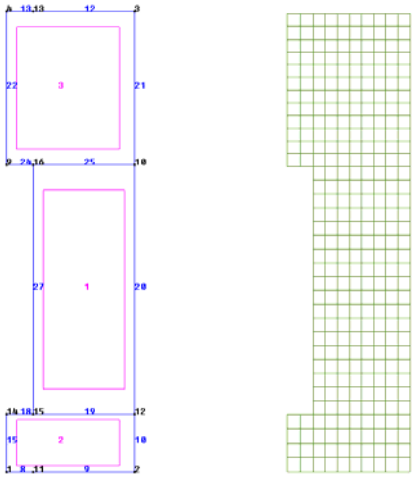

Figure 1 Geometry and mesh of the Mockup test

3 TIME STEP CONTROL

CODE_BRIGHT allows different options for time step control as is shown in Table 1. Option 1 uses a heuristic method which regulates the time stepsize on the basis of the number of iterations. Options 5 to 10 use an adaptive method which controls automatically the time stepsize based on the relative error of the variables according to a given tolerance, more restricted for the option 10. Options 1, 6, 7, 8 and 9 are employed in this study.

4 RESULTS AND DISCUSSION

A summary of the numerical performance of the model is presented in Table 2 for all options of the time step control. As it is expected, the use of a more restricted time step control (option 9) increases the number of the time-steps, computational time and total iterations of the Newton Raphson but the average number of iterations per time step is considerably reduced as the initial estimates are closer to the true solution. Table 2 indicates that the numerical performance of the heuristic method (itime=1) is similar to that incurred by the adaptive method and lies between that obtained using itime=7 and itime=8. This demonstrates that at least for this case, the heuristic scheme is capable of an efficient solution of coupled THM problems.

To examine the reliability of the solution, Figure 2(a) plots the distribution of some variables (temperature, liquid pressure and stresses) in a transversal section through the centre of the heater at the end of the simulation (2500 days). It is noted highly non-linear variations of the solutions and important discrepancies for stresses when itime=6. In the absence of an analytical solution, some surrogate “exact” solution is required for the convergence studies. The reference solution is generated by the option 9 of time step control with very tight truncation error (1e-5). A relative error of the solutions has been computed which is plotted in panel (b) of Figure 2. In general it can be observed that a decrease in the imposed error

tolerance by an order of magnitude lead to a proportional reduction in relative errors also by approximately an order of magnitude. For the temperature variable more or less uniform errors are obtained that are proportional to the requested tolerance, it is not the case for liquid pressure and stresses which can be explained by the use of highly non-linear hydraulic and mechanical constitutive laws.

ITIME = 0	**TIME STEP FACTOR IS 1.4 ALWAYS** DTIMEC is the upper bound of time step
ITIME = 1	**NUMBER OF NR ITERATIONS AS A MEASURE OF ERROR** $f = \left(\frac{4}{iter}\right)^{0.25} \geq 0.5$
RELATIVE ERROR CONTROL **First Order Approach** $0.1 \leq f = 0.8\left(\frac{DTOL}{error}\right)^{0.5} \leq \text{pdfmax}$	
ITIME = 5	DTOL = 0.1
ITIME = 6	DTOL = 0.01
ITIME = 7	DTOL = 0.001
ITIME = 8	DTOL = 0.0001
ITIME = 9	DTOL = 0.00001
ITIME = 10	DTOL = 0.000001

Table 1. Options of time step control (f is the reduction factor, pdfmax is set to 1.4)

Itime	Mean NR iterations per time step	Total NR iterations	Number of time steps	CPU time (s)
1	2.06	1674	601	84.89
6	4.10	1599	432	83.36
7	3.55	1712	539	87.83
8	1.90	2452	1043	126.31
9	1.41	5102	3050	276.30

Table 2. Summary of the numerical performance of the "Mockup test"

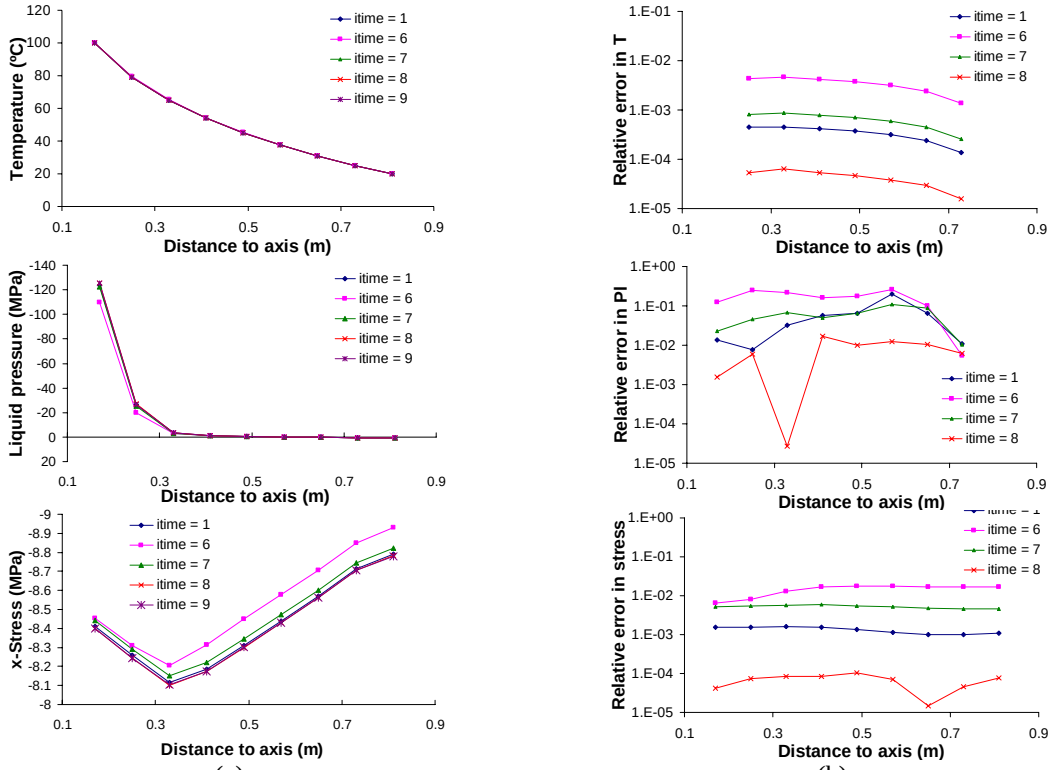

(a) (b)

Figure 2 (a) Distribution of the variables (temperature, liquid pressure and stresses) in a transversal section of the test at the final of the simulation (2500 days); (b) Relative error in the variables

The standard option assumed in CODE_BRIGHT is that variables correction in absolute values and residuals of the mass balance equations vanish in parallel when the Newton-Raphson scheme is used. In this THM example we use the option "or", which means that once the variables correction OR residuals are lower than the prescribed tolerances, the solution is

reached for each time step. Simultaneous convergence of the three variables (displacements, liquid pressure and temperature) OR the three balance equations (force, water and energy) is required to reach the solution.

The performance of the non-linear solver using the more restricted option (itime=9) and the more release option (itime=6) of the time step control is shown in Figure 3, which plots in the x-axis the simulated time and in the y-axis the error in some variables (liquid pressure and temperature) and the residual of the balance equations (water and energy). Results are plotted using different colours which correspond with a given local iteration per time step. In the problem analyzed here the convergence is reached first by the variables correction rather than by the residual of mass balance equations (for which a low tolerance of 1E-10 is prescribed). However, in both cases, a tendency of error reduction is observed. In addition, errors are small and further reduce if time stepsize is reduced, i.e., if a more restricted tolerance is employed.

Liquid pressure correction shows that for itime=9 only 3 iterations are required to satisfy the prescribed tolerance (1E-3), while, for itime=6 more than 25 iterations are required. Residual of water mass balance reaches convergence after two iterations when itime=9, while, more than 7 iterations are required to satisfied the prescribed tolerance (1E-10) when itime=6 is used. For the hydraulic behaviour both the residual of water mass balance and the liquid pressure correction are satisfied simultaneously.

Regarding temperature correction, Figure 3 indicates that for itime=9 the correction is lower than the prescribed tolerance (1E-3) after 2 iterations while for itime=6 more than 4 iterations are required. The maximum correction is up to four orders of magnitude, for itime=9, for example, the error reduces from 10^{-3} to 10^{-7} which means that the convergence by temperature is of second order. Residual of energy balance equation in does not converge, but a significant error reduction occurs that guaranties a convergence of second order.

Finally, a kind of measure of error reduction for the variables has been estimated as the ratio between the error at the iteration (i-1) and the error at the iteration (i). Table 3 presents an arithmetic mean value of the error reduction for the variables. It can be noted that the reduction factor increases as a more restricted tolerance is employed. For itime=8 the reduction factor of error is twice of that for itime=6, surprisingly, the reduction factor for itime=9 is slightly lower (with exception of temperature) than that of the itime=8. This indicates that a local truncation error tolerance of 10^{-3}-10^{-4}, that is, 0.1-0.01%, should be sufficient for most practical applications. It must also be realised that, since the numerical solution will be affected by both spatial and temporal errors, imposition of an extremely fine temporal error tolerance while employing a crude spatial grid is counterproductive.

Itime	Arithmetic mean of error reductions			
	Displacement	Liquid pressure	Temperature	Stress
1	20	21	1889	17
6	15	21	1265	12
7	19	26	1995	14
8	37	43	2808	25
9	35	29	8780	22

Table 3 Arithmetic mean of error reductions of the variables

5 CONCLUSIONS

The problem of the THM mock-up test is complex as various non-linear constitutive equations are used; however, global convergence of the problem is very satisfactory.

A local truncation error tolerance of 10^{-3}-10^{-4}, that is, 0.1-0.01%, for the adaptive method of time step control was found sufficient for most practical applications.

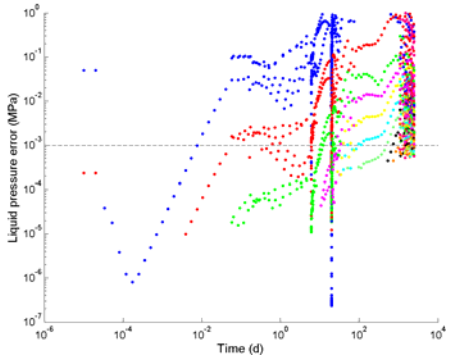

(a) Itime=6; Liquid pressure

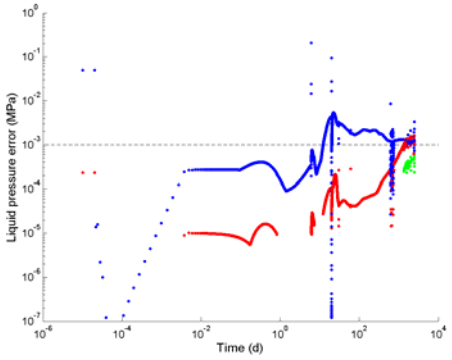

(b) Itime=9: Liquid pressure

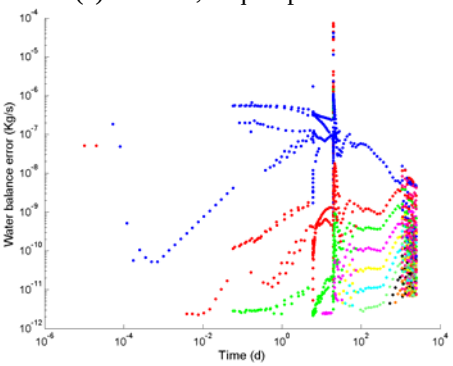

(c) Itime=6: water balance

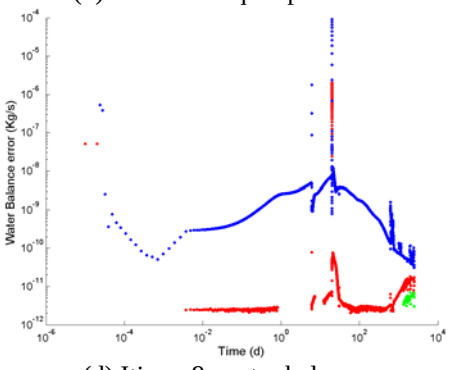

(d) Itime=9: water balance

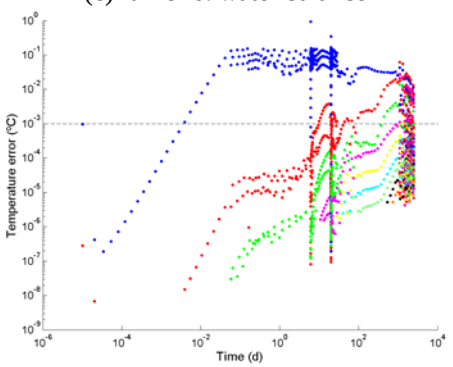

(e) Itime=6: temperature

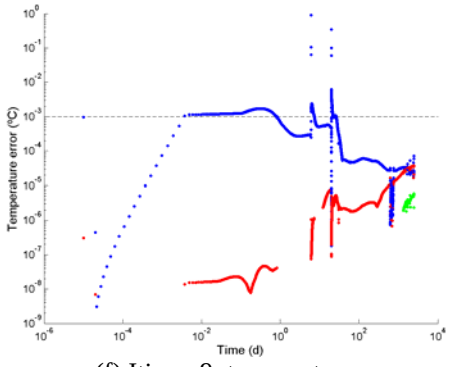

(f) Itime=9: temperature

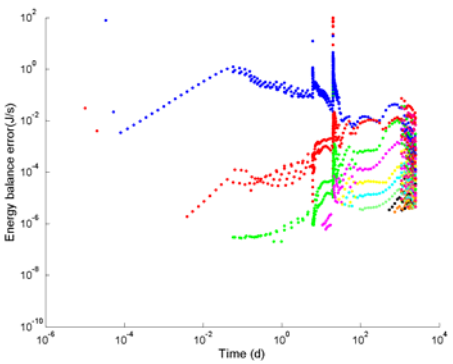

(g) Itime=6: energy balance

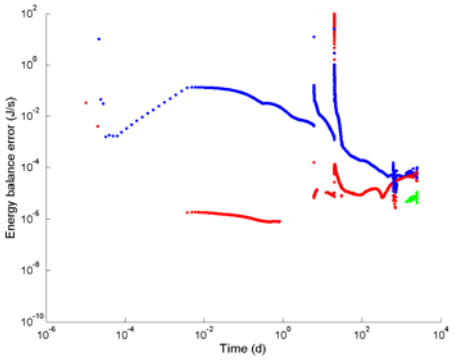

(h) Itime=9: energy balance

Figure 3 (a,b) Liquid pressure error, (c,d) residual of water balance, (e,f) temperature error, (g,h) residual of energy balance against simulated time for the options itime=6 and itime=9